File with N76-23518 REPORT

AN INVESTIGATION OF THE UNSTEADY PRESSURE FIELD WITHIN THE 8 - FOOT HIGH TEMPERATURE STRUCTURES TUNNEL

> By L. Keefe

Prepared for:

NATIONAL AERONAUTICS AND SPACE ADMINISTRATION LANGLEY RESEARCH CENTER **HAMPTON, VIRGINIA 23665**

CONTRACT NUMBER NAS1 - 12841

WYLE LABORATORIES REPORT NUMBER 50610

May 1976

SCIENTIFIC SERVICES & SYSTEMS GROUP 3200 MAGRUDER BLVD., HAMPTON, VIRGINIA

FOR NASA INTERNAL USE ONLY

RESEARCH REPORT

AN INVESTIGATION OF THE UNSTEADY PRESSURE FIELD WITHIN THE 8 - FOOT HIGH TEMPERATURE STRUCTURES TUNNEL

By L. Keefe

Prepared for:

NATIONAL AERONAUTICS AND SPACE ADMINISTRATION LANGLEY RESEARCH CENTER HAMPTON, VIRGINIA 23665

CONTRACT NUMBER NAS1 - 12841

WYLE LABORATORIES REPORT NUMBER 50610

May 1976

WYLE LABORATORIES

SCIENTIFIC SERVICES & SYSTEMS GROUP 3200 MAGRUDER BLVD., HAMPTON, VIRGINIA FOR NASA INTERNAL USE ONLY

ABSTRACT

A study of the unsteady pressure field within the combustor and test section of the NASA-Langley Research Center, 8-Foot High Temperature Structures Tunnel (HTST) has been performed. Pressure spectra and cross correlations measured at the test section centerline show fluctuations are dominated by tunnel background noise at frequencies below 5 kHz. Above 5 kHz, fluctuations display characteristics typical of pressure fields found beneath turbulent boundary layers. Further analysis of the lower frequency range for hot flow indicates a dependence of background noise on combustor conditions. Measurements within the combustor show a pressure fluctuation with components at 31 Hz and its first eight harmonics. The magnitude of this fluctuation seems to correlate well with background levels in the test section. For cold flow, the source of pressure fluctuations in the test section was not identified; however, the combustor, structural vibration, and the nozzle boundary layer were eliminated as possible sources.

In addition to the main study, the effectiveness of the model protection system in reducing startup and shutdown loads was assessed. Measurements show that loads are reduced to values close to those encountered by test articles while in the test stream.

TABLE OF CONTENTS

																												Page
INTR	RODUCTIO	N	•	•	•	•	•	•	•	•	•	•	•	•	•	•	•	•	•	•	•	•	•	•	•	•	•	1
DESC	CRIPTION	0	F	E	ΧF	Έ	RI	M	ΞN	Т						•								•		•	•	1
4	Tunnel Fa	cil	it	ÿ																								2
	Data Acqu																											
	Data Acqui																											
	Test Proc																											
	Data Analy																											
	Analysis E																											
RESU	JLTS AND	D	IS	CI	US	SI	ON	Ι.														•						6
	Test Section																											
	Combustor																											
CON	CLUSIONS		•				•		•		•	•					•	•	•	•	•		:					15
REF	ERENCES		•			•		•	•	•	•	•						•			•			•	•	•	•	17
APP	ENDIX A				•	•	•				•	•	•					•	•					•				49
APP	ENDIX B																			•								53

LIST OF TABLES

Tables		Page
I.	Summary of Run Conditions	19
II.	RMS Values of Fluctuating Pressure Measured in the Combustor and Test Section	20
	LIST OF FIGURES	
Figures		Page
1.	Overall View, 8 Foot High Temperature Structures Tunnel NASA-Langley Research Center	21
2.	General Configuration of Test Panel Holder and Test Section, 8' HTST	22
3.	Top View of Panel Holder	23
4.	Test Panel Detail and Instrumentation Locations	24
5.	Mounting Arrangement of Test Panel	25
6.	Boundary Layer Probe	26
7.	Detail of Combustor	27
8.	Data Acquisition System	28
9.	Ratio of rms Pressure to Dynamic Pressure Plotted against Mach Number. Unfiltered Data from Present Investigation	29
10.	Unfiltered Power Spectra of Pressure Compared with Results of Past Investigations	30
11.	Unfiltered Pressure Cross Correlations at Streamwise Transducer Separations \$, Cold Flow (T = 300 K)	31

LIST OF FIGURES (continued)

Figures		Page
12.	Unfiltered Pressure Cross Correlations at Streamwise Transducer Separations ξ , Run # 12 ($T_r = 1611 \text{ K}$)	32
13.	Unfiltered Space Correlations of Pressure Compared with Results of Previous Investigations	33
14.	Ratio of rms Pressure to Dynamic Pressure Plotted against Mach Number. Pressure High-Pass Filtered at 5 kHz	34
15.	Power Spectra of Pressure High Passed at 5 kHz Compared with Results of Past Investigations	35
16.	Filtered Pressure Cross Correlations at Streamwise Transducer Separations §	36
17.	Filtered Space Correlations Compared with Previous Results	37
18.	Boundary Layer Pressure (Pbl) Versus Local Dynamic Pressure	38
19.	Low Frequency Fluctuation P Versus Local Dynamic Pressure q ₁	39
20.	Comparison of Pressure Spectra Measured in the Combustor and in the Test Section	40
21.	Test, Panel Spectrum Displaying Presence of Narrow Band Noise in Hot Flow, T = 1611 K	41
22.	Combustor Spectrum, T _r = 1611 K	42
23.	Comparison of Combustor and Test Section Spectra for Cold Flow, T = 300 K	43
24.	Comparison of Low Frequency Spectra from Combustor and Test Section in Cold Flow, T _r = 300 K	44

LIST OF FIGURES (continued)

Figures		Page
25.	Test Section Pressure Fluctuations below 5 kHz Correlated with Combustor Pressure Variations	45
26.	Ratio of Unsteady to Steady Combustor Pressure $\frac{\text{comb}}{P_r}$ Plotted against Steady Combustor Pressure	46
27.	Combustor Pressure Ratio $\frac{P_{comb}}{P_{r}}$ Plotted Versus Combustor Total Temperature	47
28.	Combustor Spectrum Measured during Tunnel Operation with a Cracked Fuel Spray Bar, T = 1450 K	.48
Al.	Position of Acoustic Baffles/Model Protection System	50
A2.	Comparison of rms Pressure Time Histories Measured on the Test Panel during Tunnel Startup and Shutdown	51
A3.	Comparison of rms Pressure Time Histories Measured on the Test Panel during Tunnel Startup and Shutdown	52
B1.	Ratio of rms Pressure to Dynamic Pressure Plotted against Mach Number. Results of Previous Work	59
B2.	Power Spectra of Pressure Fluctuations from Previous Investigations	60
В3.	Pressure Cross Correlation beneath Turbulent Boundary Layers at Various Transducer Separations ξ	
B4.	Pressure Cross Correlations beneath Turbulent Boundary Layers at Various Transducer Separations ξ	62
B5.	Pressure Space Correlation from Previous Investigations	63

SYMBOL TABLE

G (ψ)	Power Spectral Density
L	Correlation Length
1	Characteristic dimension of a turbulent flow
M_1	Local Mach Number
M _w	Free Stream Mach Number
p(x, t)	Pressure at location x and time t
P _{bl}	RMS value of boundary layer dominated pressure fluctuations at frequencies above 5 kHz
P	RMS value of combustor pressure fluctuations
P	Combustor Total Pressure
P _{tot}	Total rms value of pressure fluctuations measured on plate surface
Pu	RMS value of pressure fluctuations at frequencies below 5 kHz
$\mathbf{q}_{\mathbf{l}}$	Local dynamic pressure
q_{ω}	Free Stream dynamic pressure
R(ξ)	Space Correlation function
R _ξ (τ)	Cross Correlation Function of two points ξ apart in the streamwise direction
Tr	Combustor Total Temperature
U	Characteristic velocity in a turbulent flow
U _c	Convection velocity of turbulent eddies
\mathbf{U}_{1}	Local velocity
ບູ	Free Stream Velocity
α	Model Angle of Attack
δ^{*}	Boundary layer displacement thickness
ξ	Separation distance in streamwise direction
ė	Boundary layer momentum thickness
T T	Time Delay
ω .	Circular frequency

INTRODUCTION

The first flights of most airplanes and aerospace vehicles have been preceded by development programs which included many hours of scale model wind tunnel testing. To apply the information obtained from such tests to full-scale vehicles, however, there must be some assurance that a correct reproduction of actual flight conditions has been achieved. Unsteady flow, which exists to some extent in all wind tunnels, is a possible source of error in such testing. By just its influence on boundary layer transition, unsteady flow can affect measurements of steady lift and drag as well as heat transfer.

With such possibilities it is advisable to assess the flow quality within a wind tunnel in order that sources of measurement error can be identified and, if possible, eliminated. The investigation embodied in this report examines the unsteady pressure field within the 8-foot High Temperature Structures Tunnel (HTST) at NASA-Langley Research Center for this purpose.

Over portions of a vehicle's surface where the flow is attached and shock-free in flight, pressure fluctuations can result only from the turbulent boundary layer covering it. The presence of other fluctuations during tunnel testing represents a possible source of error. This differentiation between boundary layer and nonboundary layer sources of pressure fluctuations provides a natural means of identifying spurious contributions to the pressure field within a tunnel. Deviations from the well documented behavior of boundary layer pressures will confirm the presence of these contributions while the specific character of the deviations should provide information on their source.

With such an analysis in mind, overall levels, power spectra and cross-correlation functions of pressure measured in the test section are presented. Using these, the frequency range over which spurious fluctuations dominate is bracketed, and some identification of sources is carried out.

As a sidelight to the main study, the effectiveness of the HTST model protection system in reducing startup and shutdown loads was measured. The results of this investigation are presented in Appendix A.

DESCRIPTION OF EXPERIMENT

Using a longitudinal line of pressure transducers flush mounted in a flat

plate, the fluctuating pressure field inside the test stream of the HTST was measured for a variety of tunnel operating conditions and two model angles of attack (0°, -15°). Concurrently with these measurements, conditions within the tunnel combustor section were monitored with a single pressure transducer. Boundary layer profile information for the flat plate was derived from traverses of a pitot pressure/total temperature probe. Fluctuating pressure data were recorded on magnetic tape and later analyzed to determine their rms values, power spectra, and cross-correlation characteristics. A description of the HTST facility, data acquisition and analysis procedures, and the instrumentation employed in the test program is provided in the following paragraphs.

Tunnel Facility

The experimental measurements took place in the 8-ft HTST at Langley Research Center. The 8-ft HTST is a hypersonic, blowdown tunnel with an open jet test section 2.44m (8 ft.) in diameter and a nominal test section Mach number of seven. General details of the tunnel are shown in Figure 1. fluid of the tunnel is methane-air combustion products. Reservoir conditions in the combustor range in temperature from 1366 K to 2367 K (2000°F to 3800°F) and in pressure from 6.894 x 10^6 N/m² to 2.758 x 10^7 N/m² (1000 psi to 4000° psi). If desired, reservoir temperatures in the range of atmospheric conditions (300 K) may be obtained by operating the tunnel without combustion. cles are attached to a retractable sled which can be pitched to angles from -20° to +20° with respect to the tunnel centerline. Table I contains a listing of the conditions at which the tests in this series were performed. The tabular values of local velocity (U_1) , dynamic pressure (q_1) , and Mach number (M_1) were measured above the test sled surface outside the boundary layer. Free stream values (U, q, , M) may be determined using oblique shock relations. Depending on air supply, test conditions, and nozzle cooling requirements, run times varied from 30 to 70 seconds. Further information on the performance characteristics of the 8-ft HTST may be found in Reference 1.

Data Acquisition Program

The essential pressure and boundary layer measuring devices were four piezoelectric pressure transducers flush mounted in a flat plate and a remotely operated pitot pressure/total temperature probe. These instruments were mounted on the tunnel's test panel holder which was injected into the test section when steady flow conditions had been established and retracted when data recording was complete. General details of the tunnel test section and panel holder are shown in Figure 2. Specific dimensional information on transducer locations is shown in Figures 3 and 4.

The transducers were flush mounted in a 45.7cm x 33.0cm x 2.5cm (18" x 3" x 1") aluminum plate. Vibration dampers provided shock isolation between the plate and the panel holder. A photograph of the plate, showing the positions of the dampers, is presented in Figure 5. The plate itself was also instrumented with an accelerometer and two thermocouples to measure the acceleration and temperature environments experienced by the pressure transducers. In addition, static pressure on the plate was measured through a port 7.62cm (3") off the center line at the same axial station as the third pressure transducer.

A boundary layer trip, consisting of a row of 2.39mm (0.094") diameter spheres, 9.55mm (0.374") apart, was located 12.75cm from the leading edge of the panel holder. Reference 1 indicates that this should have produced a fully developed turbulent boundary layer at the transducer locations in all runs except No. 4. Transitional flow was expected for this one exception. Two-dimensional flow over the panel holder was achieved by attaching side plates extending both above and below the panel holder's surfaces.

The boundary layer probe, pictured in Figure 6, was mounted 174.6cm from the leading edge of the panel holder. The sensing elements consisted of a pitot pressure probe made from stainless steel tubing 1.65mm (0.065") in diameter and a platinum-platinum rhodium 13% total temperature thermocouple. The probe required approximately three seconds to complete a vertical cycle (upstroke, downstroke) and extended 7.62cm (3") above the model surface at the top of its stroke. Boundary layer parameters listed in Table I occurred at the axial station of the probe. Extrapolation of these values upstream to the first transducer position was accomplished using the methods described in Reference 2.

In addition to the instrumentation in the test section, a single pressure transducer was placed in the tunnel combustor, upstream of the fuel spray bar, to record the level of pressure fluctuations. The general location of this transducer is indicated in Figure 7.

Data Acquisition Instrumentation

The outputs of all test section transducers were recorded on magnetic tape for later analysis. Accelerometer and pressure transducer outputs were amplified prior to recording. Thermocouple outputs as well as boundary layer measurements were digitized at twenty samples/second and recorded in the tunnel control room. A block diagram of the data acquisition equipment is

shown in Figure 8. Major system components are described in the following paragraphs.

Pressure Transducer (PCB 112M44). The pressure transducers employed in the test panel were quartz crystal, piezoelectric devices having a nominal sensitivity of 50 mV/psi. Their frequency response was ±3 dB from 10 Hz to 100 kHz and the diameter of their active sensing area 3.81mm (0.150"). In the present application, the transducers were mounted in water-cooled adapters (PCB 64A02) and recessed 0.127mm (0.005") below the test panel surface. The recess was filled with General Electric RTV 560 silicone rubber to reduce heat transfer to the crystal through the diaphragm and to decrease any pyroelectric effects due to unsteady temperature variations in the tunnel. The thin layer of rubber had no noticeable effect upon the frequency response of the transducers.

Scaling arguments based on the results of previous boundary layer investigations (Refs. 3-8) indicate the probable presence of pressure fluctuations at frequencies as high as 300 kHz within the boundary layer developed in the 8-ft HTST. There are, unfortunately, no commercially available transducers of sufficient sensitivity with response this broad. A previous NASA study (Ref. 3) conducted at conditions similar to those encountered in the 8-ft HTST, employed a transducer developed specially for that application. The response of this transducer extended from 1 kHz to 300 kHz. However, subsequent analysis showed that the energy measured above 100 kHz had negligible effects upon calculated overall pressure levels and boundary layer characteristics. For this reason the response of the PCB 112M44 transducer was regarded as adequate for this investigation.

<u>Pressure Transducer (PCB 113A24).</u> Measurements of fluctuating presure within the combustor were obtained with this quartz crystal transducer. Its full-scale range was $6.89 \times 10^6 \text{ N/m}^2$ (1000 psi) at a nominal sensitivity of 5 mV/psi. Crystal resonance is specified by the manufacturer as in excess of 500 kHz.

Accelerometer (PCB 302A). The acceleration level of the plate was measured with this unit. This is a quartz, piezoelectric device, with a flat response from 5-5000 kHz, and is capable of operation at temperatures to 395 K.

Battery Power Supply (PCB 480A). Each power supply provided a constant 18 volt, two milliamp excitation current to a single pressure transducer or accelerometer. They were used in preference to line power supplies because of their low noise characteristics.

Thermocouples. Standard chromel-alumel thermocouples measured test panel temperatures. They were mounted at the top of holes counterbored to within 3.175mm (0.125") of the plate surface. Contact between the thermocouples and the aluminum was maintained by spring pressure.

Amplifiers (Neff 122). The outputs of the plate pressure transducers and the accelerometer were amplified by these units prior to recording onto magnetic tape. They were wideband, differential dc amplifiers which produce gains from 0 to 1000 in eleven fixed steps with an additional variable gain from 1 to 2.5 at each fixed step. At all values of gain, their frequency response is +3 dB from dc to 100 kHz.

Tape Recorder (Sangamo Sabre 3). This is a standard 14-channel instrumentation tape recorder. When supplied with FM wideband group 1 electronics and operated at 305 cm/sec (120 ips) it has a flat frequency response from dc to 80 kHz on all channels.

Pressure Transducer Calibrator (Photocon PC 125). Prior to each tunnel run, this unit was used to check the sensitivity of each pressure transducer in the test section. It contains an oscillator, power amplifier, and portable driver which will produce a 1000-Hz signal in a continuously adjustable range from 100 dB to 160 dB (re 0.00002 N/m²). The frequency of the calibration signal may be varied through an external oscillator connection, though at the cost of decreased sound pressure level for lower frequencies. Using this connection, sensitivity checks were performed at 250 Hz and at either 130, 140, or 150 dB.

Test Procedure

Prior to each tunnel run; the sensitivity of the pressure transducers was checked by placing the portable driver from the acoustic calibrator over each unit and recording the resultant voltage due to a known sound pressure level on tape.

Data recording began with pilot burner ignition in the combustor and continued until final shutdown of the tunnel after the model was retracted. Thus, both the transient pressure loading associated with tunnel starting processes as well as the pressure fluctuations beneath the boundary layer during steady flow were measured.

Data Analysis Procedures

Tape records of pressure and acceleration time histories were analyzed

after each run in terms of overall levels, power spectra, and cross correlations between various pairs of pressure transducers. No correction of the pressure records for transducer acceleration sensitivity was required. Spurious signal levels generated by acceleration were more than 15 dB below the recorded pressure levels at all frequencies. Numerical integration of the digitized temperature and velocity yielded the boundary layer parameters used to scale both spectra and correlation functions. Data were first analyzed without any filtering of low-frequency data and subsequently reanalyzed with high pass filtering at 5 kHz to demonstrate the effect this had on both overall levels and the correlation functions.

Analysis Equipment

Spectrum Analyzer and Averager (Federal Scientific UA-14 and 1014).

Power spectra of pressure fluctuations were obtained with this device. Its
400-point resolution can be applied over frequency ranges from 0-10 Hz to
0-50 kHz for a real-time analysis. For recorded signals, the effective analysis range may be increased by playing the tape at some fraction of its recording speed. The highest frequency analyzed then becomes a product of the total analysis bandwidth set on the machine multiplied by the reciprocal of the tape speed fraction. In this manner, the pressure data was analyzed to 100 kHz by playing the tape records at half speed and using the 0-50-kHz range of the analyzer.

Correlator (SAICOR 43A). This instrument accepts dual inputs, A and B, and will calculate either the autocorrelation $R_{AA}(\tau)$ or the cross correlations $R_{AB}(\tau)$ or $R_{BA}(\tau)$. Correlations at time delays as small as 200 nanoseconds may be determined. Mean square values of random signals can be determined by computing their autocorrelation function and calculating its value at $\tau=0$. This method was used to determine overall pressure levels and accelerations.

<u>Filters (Krohn-Hite 3202).</u> These units are solid-state high- and low-pass filters with continuously adjustable cutoff frequencies from 20 Hz to 2 MHz. In their maximally flat response mode, they are -3 dB at the cutoff frequency and provide 24 dB/octave attenuation outside the pass-band. They were used to filter the pressure records prior to the second analysis of this data.

RESULTS AND DISCUSSION

During testing and subsequent data analysis, primary importance was placed on describing the unsteady pressure field within the test section of the HTST. However, the demonstrated effect which combustor pressure had upon

test section conditions naturally led to an additional study of the combustor environment. The analysis in the following sections parallels this emphasis, consideration being given primarily to test section conditions with an analysis of the combustor included as an aid to understanding these conditions.

Test Section

Several mechanisms exist that could cause pressure fluctuations on the surface of an object in the test section of the HTST. Among these are acoustic radiation from the combustor and nozzle boundary layer, flow oscillation due to total pressure changes upstream of the nozzle throat, and turbulent boundary layers covering the object. Because of the Mach number of the nozzle exit flow, there is no possibility that turbulence generated noise (jet noise) radiating from the jet mixing region can reach the tunnel centerline within the test section.

From the viewpoint of reducing measurement errors, it would be desirable to eliminate all pressure fluctuation mechanisms except the turbulent boundary layer. Since a boundary layer will be present on vehicles in flight, it is the only "natural" mechanism and should be present during testing. It is this division between boundary-layer and nonboundary-layer mechanisms which provides criteria for analyzing the data in these tests. Deviations of the pressure field behavior from that of a turbulent boundary layer will confirm the presence of additional sources of fluctuation. Further analysis of the specific character of these deviations should then give some indication of which source was their cause.

The behaviour of the pressure field beneath turbulent boundary layers is well documented (Refs. 3-8). The random convecting pattern of turbulent eddies which causes the velocity perturbations within the boundary layer carries with it an associated random pressure field. As the identity of an eddy decays under the influence of shear, viscosity, and diffussion, so does its associated pressure field. The random nature of the field necessitates that its description be of a statistical nature. Explanations of the statistical measures frequencly used in this description are given in Appendix B, along with results from past boundary layer investigations (Refs. 3-8) which demonstrate their physical interpretation. Briefly, the root-mean-square (rms) value is a convenient measure of the average dynamic amplitude of the pressure fluctuations, while the power spectrum specifies their frequency content and the space-time-correlation function their temporal and spatial coherency. A more rigorous discussion of these parameters is found in Reference 9.

Power spectra, rms values, and correlation functions were computed from the pressure data measured in the test section. A comparison between this data and results of previous boundary layer investigations (cited in Appendix B) displays substantial differences, indicating the presence of a source of pressure fluctuations other than the boundary layer.

RMS Values. In Figure 9, the rms pressures measured on the plate are plotted along with the results from previous investigators. Except in comparison to the results of Chen, the pressure levels for this test range from two to five times those measured in other experiments within the same Mach number range. However, due to the large scatter of data from other investigations, no decisive importance can be attached to this discrepancy.

Power Spectra. In Figure 10, power spectra of pressure fluctuations measured in this experiment are compared to the results of five other investigations. The spectra, newly plotted, come from the single cold flow run (No. 11) performed and a hot run (No. 12) which displays flow characteristics typical of all hot runs (except No. 4, when flow over the transducers was transitional). Several areas of disagreement stand out in this comparison. Previous investigators have established the spectrum of boundary layer pressure fluctuations to be broadband, as one would expect for a quantity whose time history is random. Here, the measured spectra are broadband at high frequencies $(\frac{\omega \cdot \delta^*}{U_1} > .4)$, but contain discrete frequency components and narrow bands of noise whose amplitude rises considerably above the broadband level at low frequencies. In the cold flow case, four narrow bands of noise occur, centered at 56, 420, 1250, and 3600 Hz. In each case, the amplitudes within these bands rise to values twenty to fifty times larger than the broadband level expected in this region. For the hot flow case, two of the four bands of noise reappear (though they are shifted on the plot because of the different values of $\frac{\delta^*}{U_1}$ in the two runs) and at very low $\hat{\mathbf{frequencies}}$ the spectrum is dominated by peaks at 31 Hz and its first eight harmonics. This divergence from broadband behavior indicates that the pressure field is not random in either hot or cold flow.

While the bands of noise and discrete frequencies occur at low frequencies, the high-frequency portions of the spectra also show discrepancies with previous work. The shape of the spectrum appears generally correct in this region (with the characteristic high-frequency roll-off) but amplitudes are considerably lower than those measured by other investigators. However, this feature can be traced directly to the previous discussion of the rms values and the particular way in which the spectral curves are plotted. Note that the power spectra G(w) are normalized by the ratio P^2 / q^2 . This is just the square of the values P tot q^2 plotted in Figure 8, where they were noted to be slightly high compared to previous results. Normalization by this higher ratio leads to low spectral values and the suspicion arises again that the values P /q are incorrectly high.

Certainly if their values were reduced, the magnitude of the high-frequency components in the spectrum would fall closer to those found in previous investigations.

Cross-Correlation Function. Cross-correlation functions measured between the leading three transducers are displayed in Figures 11 and 12 for both the cold and hot flow runs. Their most striking characteristic is their periodicity, a feature absent from results of previous investigations (see Figures B-3, 4). Instead of peaking at a single time delay corresponding to eddy travel time between transducers, these cross correlations peak at regular intervals and little decay of the peak value occurs. In this situation, it is difficult to define a convection velocity. The periodic nature of these plots further confirm that the pressure field repeats itself in time rather than fluctuating randomly. In the cold flow case the correlation function peaks at intervals of approximately 800 µsec, which corresponds to the period of 1250 Hz, the center frequency of one of the narrow bands of noise in the spectra. For hot flow, the correlation function repeats itself at intervals corresponding to the period of 31 Hz, the fundamental discrete frequency already noted in the spectrum for that and all other hot flow runs.

Space Correlation. Space correlation functions for the representative hot and cold runs are plotted in Figure 13. The solid lines are the envelope of space correlation curves displayed in Figure B-5 from other boundary layer studies.

While the cold flow correlation function seems to be in reasonable agreement with previous work, the function measured in hot flow is quite different. Instead of falling monotonically to a slightly negative value, and then going asymptotically to zero as transducer separation increases, the curve stays positive over the entire measurement range and performs a small oscillation. Because no measurements of space correlation were made at greater transducer separation, it is impossible to say whether the correlation function goes to zero or remains positive for larger distances. However, even without this information, it is apparent that the correlation length defined by this curve must be considerably larger with respect to δ^* than those measured in previous work. There $L \approx 3\delta^*$, whereas here L equals at least $8\delta^*$. If there is little or no change in the correlation scale in the transverse direction, the correlation area for the hot flow case is about two and one-half times larger than expected.

Evaluation of Results. The magnitude, spectra, and correlation functions computed from the pressure data all indicate substantial deviations from the characteristics of a turbulent pressure field. The pressure magnitudes are too high, the power spectra are dominated by discrete frequencies or narrowband noise, and the correlation functions indicate that the pressure field no

longer has a random character in time. The pressure correlation areas are probably too large, and it is difficult to define either the convection or decay of the pressure field.

The key to identifying the cause of these deviations lies in the power spectra. They divide into two parts: a low-frequency region ($\frac{w\delta^*}{U_l}$ < .4) dominated by narrow-band noise and discrete frequency components, and a high-frequency region with the broadband character and roll-off associated with a turbulent boundary layer spectrum. It seems probable that the two parts of the spectrum are due to different sources of fluctuation. To test the hypothesis that the high frequency components were indeed due to a turbulent boundary layer and that their characteristics were being masked beneath the low-frequency fluctuations, the data was reanalyzed after being high-pass filtered at 5 kHz to remove the lower portions of the spectrum. A frequency of 5 kHz was chosen so that the highest frequency narrow band of noise (at 3600 Hz) would be attenuated below the broadband level of the remaining portion of the spectrum.

The results of this second analysis are presented in Figures 14, 15, 16, and 17. Comparison with data from previous boundary-layer investigations, (Figures B-1 to B-5), now shows substantial agreement. Filtered rms pressure magnitudes occupy a central position within the scatter of data at those Mach numbers, power spectra have not only the approximate shape but also the magnitude found in previous work, cross-correlation functions display the characteristics of a random pattern with well defined convection speed and decay, and space correlation functions now show a pattern of pressure which is coherent over nondimensional distances ξ/δ^* compatible with boundary layer phenomena.

The general picture, indicated by the two analyses of the pressure data, confirms that pressure fluctuations at frequencies higher than 5 kHz are dominated by the turbulent boundary on the plate while those fluctuations at lower frequencies are dominated by other sources of pressure fluctuation in the tunnel. Insight into the behavior of these other sources can be gained from further analysis of the lower? frequency region.

In all probability, several different mechanisms contribute to the lower frequency fluctuations. The influence of the boundary layer extends into this region, but is obviously masked due to the large magnitudes of the other sources. There is no particular frequency in the spectra at which a sharp dividing line can be drawn between the boundary layer fluctuations and the other sources.

Instead, a gradual transition occurs from a frequency region where the boundary layer dominates to a region where the unknown sources dominate. Frequencies near 5 kHz represent the lowest border of the region where the boundary layer is the dominant source of fluctuation.

With this in mind, the total fluctuation of pressure P_{tot} in the test section will be divided into two parts: P_{bl} , composed of the boundary layer dominated fluctuations above 5 kHz, and P_{u} , composed of fluctuations from all sources below 5 kHz. In Table II, rms values of P_{tot} , P_{bl} , and P_{u} are given for most of the runs. They represent the average of values measured at the first two transducers (data from the third and fourth were sometimes contaminated by a crystal resonance problem).

As Figure 18 demonstrates, P_{bl} seems to scale on q_l , a behavior found in previous boundary layer studies. The low frequency fluctuations P_u shows a similar behavior in Figure 19 but the scatter about the trend line is quite large. A plot of P_u against M_l shows no apparent relation between the two parameters and is thus not displayed. Generally, the behavior of P_u shows little dependence on variation of test section conditions, indicating that its sources are probably somewhere else.

The discrete frequency and narrow band processes which dominate P, would seem to exclude a variety of aerodynamic sources from consideration as the controlling mechanism. Except at very low Reynolds numbers, and in acoustic feedback situations, aerodynamic noise sources do not display discrete frequency behavior. Reynolds numbers here are beyond the sensitive range. Feedback situations require subsonic flow somewhere to allow acoustic excitation to propagate back to the source of disturbances, and at no location downstream of the nozzle throat is this condition met except in a thin layer close to the nozzle wall. Sound waves propagating upstream within this layer will be refracted into the supersonic flow by the severe velocity and temperature gradients and then swept downstream. Thus, no feedback loop could operate in these conditions. A further argument against an aerodynamic source for at least the narrow-band noise lies in the apparent invariance of the band center frequencies in substantially different flow conditions. The spectra of aerodynamic sources scale on the ratio U/l, where U is a typical velocity, and 1 a typical length scale in the generating flow. Increasing the flow velocity j should shift the spectrum to higher frequencies while increasing length scale should lower them. From Run 11 to Run 12, the velocities increase almost threefold, yet no shift in the noise bands occurs. The possible change in length scale between the two runs is not enough to cancel this effect. It is still possible that the nozzle boundary layer could be radiating the broadband

portion of P_u, but the dominant discrete frequency components must emanate elsewhere.

Another possible source for the narrow band and discrete frequency fluctuations which must be eliminated is sound radiation from the structure of the nozzle. Complex structures with real edge conditions do not resonate at evenly spaced harmonics. Though the structure is undoubtedly excited by the nozzle boundary layer, it could not radiate the discrete frequency sound at 31 Hz and its harmonics. As far as the narrow band noise goes, more than four natural modes of vibration exist for the nozzle below 4000 Hz, and it seems unlikely that the uniform excitation by the boundary layer in this frequency range should cause response only in these four modes.

Pressure spectra measured in the combustor show strong fluctuations at 31 Hz and its harmonics, identifying this location as the source of the discrete frequency components. Values of rms pressure fluctuation within the combustor are included in Table II under the heading $\mathbf{P}_{\text{comb}}.$ In Figure 20*, a spectrum of pressure fluctuations within the combustor from 0-300 Hz for $T_r = 1611 \text{ K} (2440^{\circ} \text{F})$ is compared with the spectrum of fluctuations measured during the same run at the first transducer in the panel holder. Except for the peak at 155 Hz, each peak in the test section spectrum corresponds to a peak in the combustor spectrum. A similar comparison exists in all other hot flow runs. Unfortunately, the combustor spectra reveal little about the origins of the narrow band noise. In Figure 21, a test section spectrum for $T_r = 1611 \text{ K}$ covering 0-5 kHz shows the presence of the narrow band noise at 420, 1250, and 3600 Hz, while in Figure 22, a combustor spectrum from the same run for 0-500 Hz does not show the presence of any narrow band noise at 420 Hz. No combustor spectra from 0-5 kHz were obtained for any hot run so the absence of the bands at 1250 and 3600 Hz is conjectural. However, in the cold flow run, data recorded in both combustor and test section were analyzed from 0-5 kHz and the comparison of these two spectra in Figure 23 shows narrow band noise in the test section but none in the combustor of corresponding fre-

^{*}The vertical scale in Figures 20-24 and 28 corresponds to 10 dB SPL per inch. However, this holds true only for the first 20 dB below the peak of each spectrum, due to the limited linear dynamic range of the spectrum analyzer. Below this the vertical scale is nonlinear for each spectrum. Figures 9 and 14 have been plotted taking this nonlinearity into account, but no compensation has been applied in 20-24 and 28 as only qualitative comparisons are being made.

quency. The apparent matching of peaks in the two spectra at the lowest frequencies is a result of the inadequate resolution of the analyzer in the 0-5-kHz range. Figure 24 shows this feature in the combustor spectrum to consist of two peaks, with the test panel peak at 56 Hz falling between them.

This evidence does not completely exclude the combustor as the source of these bands, however. Based upon the manufacturer's specifications, the combustor pressure transducer was unable to detect pressure changes smaller than 0.015 psi, or 134 dB sound pressure level. Fluctuations as small as 129 dB are large enough to cause the measured levels of narrow band noise in the test section if only attenuation of the sound due to wavefront spreading during expansion in the nozzle is considered. Thus, the narrow band noise may be present, but at a level below the noise floor of the transducer.

Since the correspondence between the discrete frequency fluctuations in the combustor and test section seems established by Figure 20, it is reasonable to expect that the magnitude of P_u will depend upon P_{comb} , the magnitude of pressure flucutations in the combustor. In Figure 25, P_u is plotted against P_{comb} for the seven runs where values of both are available. Even with this limited information, P_u shows a definite increase as the combustor fluctuations increase. The lowest value of P_u is that measured during cold flow. Its appearance close on the trend line established by the hot flow data is probably coincidental. It should be remembered that Figure 23 shows little relation between combustor and test section fluctuations for cold flow.

Combustor

In hot flow, discrete frequency combustor pressure fluctuations are the major source of undesirable unsteady pressure variations in the test section. The key to understanding test section behavior thus lies in further study of combustor oscillations and their relation to tunnel operating conditions.

Values of rms combustor pressure oscillation appear in Table II. In Figure 26, the ratio of fluctuating to steady combustor pressure, $\frac{P_{comb}}{P_{r}}$ is plotted versus P_{r} . Except for data taken during two runs (Nos. 18 and 19), when the fuel spray bar cracked, this ratio remains relatively constant at $\frac{P_{comb}}{P_{r}}$

1.7 x 10^{-2} . The effect of varying the total temperature within the combustor at

constant total pressure upon this ratio is inconclusive. Figure 27 shows an increase of $\frac{P_{comb}}{P_{r}}$ with temperature for $P_{r} \simeq 6.8 \times 10^{6} \text{N/m}^2$, but a decrease

with temperature for $P_r \simeq 17 \times 10^6 \text{N/m}^2$. The limited temperature range encompassed by the data makes conclusions on this subject hazardous. Thus, the magnitude of combustor fluctuation appears to depend mainly upon the combustor pressure; the fluctuation magnitude increases linearly as the total pressure does.

Combustor fluctuations increase markedly when the fuel spray bar is broken. Visual monitoring of the pressure waveform in these conditions also shows it to be more impulsive in character than that generated during operation with an unbroken spray bar. The power spectra measured during these runs display a much greater density of discrete frequency components and asharmonic structure which extends to at least 1000 Hz. A combustor spectrum, measured during such conditions (Run 19) is shown in Figure 28. Here, there appear to be recognizable peaks every 15-16 Hz across the spectrum. The 31-Hz component still has the largest amplitude but energy at approximately 110, 142, and 248 Hz is quite prominent.

The appearance of discrete frequency pressure fluctuations within combustion chambers is a problem often encountered in rocket engine development. Reference 10 gives a comprehensive review of the analysis and engineering techniques commonly used to solve such problems. The fundamental frequency (31 Hz) of the pressure in this case places it in the class of intermediate to high-frequency fluctuations as defined in this reference. High-frequency fluctuations are generally attributed to excitation of acoustic resonances in a combustion chamber. Intermediate frequency disturbances do not occur at acoustic resonance points but seem to involve coupling of non-resonant wave motion in the chamber with fueldsystem dynamics. (Low-frequency phenomena are defined by conditions when the wavelength of interest is much larger than typical chamber dimensions. Such is not the case here.) Acoustic resonance seems to be the most likely mechanism in this case. Calculation of the fundamental oscillation mode of the combustor, taking into account the different temperatures upstream and downstream of the spray bar, gives values from 30.5 to 33 Hz for the temperature range displayed by T_r in Table I. damental frequency should vary with combustor temperature, but no consistent trend can be found in the combustor spectra from the hot runs because the uncertainty in determining this frequency from the spectra is somewhere between 1 and 1.5 Hz. Discovery of such a trend would further confirm the acoustic resonance hypothesis.

The spectral structure of the combustor fluctuations during operation with a cracked spray bar is not consistent with the acoustic resonance mechanism likely during normal conditions. The appearance of energy at 15-16 Hz and its odd harmonics is not compatible with the possible standing wave patterns within a cylinder closed at both ends. The resonance mechanism does provide an explanation of the increased amplitude of the fluctuations, however. The amplitude of fluctuations during normal operations are certainly sufficient to cause structural vibration in the rings of the spray bar. When a crack appears, this flexing of the structure will cause the open area of the cracks to vary periodically. The methane spilled through the cracks will then also oscillate and local combustion processes will follow the supply of fuel. This will feed additional energy back into the pressure oscillations and complete the loop.

CONCLUSIONS

The unsteady pressure field sensed on the surface of articles placed in the test stream of the 8-ft HTST is separable into two frequency regions within which different sources of pressure fluctuations dominate. Above 5 kHz, pressure fluctuations are attributable to the turbulent boundary layer on the article; below this frequency, tunnel background noise is the dominant source. Though the bandwidth of the background noise is limited, the total fluctuation energy contained in this frequency region is from two to eighteen times larger (depending upon flow conditions) than the energy contained in the boundary layer fluctuations. Thus, the overall character and behavior of the unsteady pressure field is controlled by the low frequency background noise levels.

Under hot flow conditions, the majority of interfering noise originates in the combustor. Excitation of the fundamental acoustic resonance of the combustor by the combustion process results in large amplitude (20-40 psi rms) discrete frequency pressure fluctuations at approximately 31 Hz and its first eight harmonics. These are transmitted to the test section and are dominant in the low frequency background noise.

In both cold and hot flow, the sources of four large amplitude, narrow bands of noise have not been identified. Combustion, structural resonance, and turbulence generated noise have been eliminated as possibilities. Sound radiation from within the air supply system is also an unlikely source, though a question exists whether the transducer within the combustor had sufficient sensitivity to detect such noise.

The magnitude of combustion induced pressure fluctuations depends mainly upon the total pressure. The ratio of combustor fluctuating pressure to total pressure remained roughly constant at 1.7 x 10^{-2} for total temperatures ranging from 1259 K (1806°F) to 1889 K (2940°F).

The model protection system reduces unsteady pressure loads encountered during normal startup and shutdown procedures by a factor of approximately 3. Fluctuating pressure levels are still high, but do not exceed those the model encounters while in the tunnel test stream. Details are presented in Appendix A.

REFERENCES

- 1. Deveikis, W. P.; and Hunt, L. R.: Loading and Heating of a Large Flat Plate at Mach 7 in the Langley 8-Foot High Temperature Structures Tunnel. NASA TN D-7275, 1975.
- Miner, E. W.; Anderson, E. C.; and Lewis, C. H.: A Computer Program for Two-Dimensional and Axisymmetric Nonreacting Perfect Gas and Equilibrium Chemically Reacting Laminar, Transitional and-or Turbulent Boundary Layer Flows.
 VPI-E-71-8, Virginia Polytechnic University, May 1971 (See also NASA CR 1893).
- 3. Raman, K. R.: A Study of Surface Pressure Fluctuations in Hypersonic Turbulent Boundary Layers. NASA CR-2386, 1974.
- 4. Speaker, W. V.; and Ailman, C. M.: Spectra and Space Time Correlations of the Fluctuating Pressures at a Wall beneath a Supersonic Turbulent Boundary Petrubed by Steps and Shock Waves. NASA CR-486, 1966.
- 5. Serafini, J. S.: Wall-Pressure Fluctuations and Pressure-Velocity Correlations in a Turbulent Boundary Layer. NASA TR R-165.
- 6. Willmarth, W. W.; and Woodridge, C. E.: Measurements of the Fluctuating Pressure at the Wall beneath a Thick Turbulent Boundary Layer. J. Fluid Mech., Vol. 14, 1962, p. 187.
- 7. Bull, M. K.: Wall Pressure Fluctuations Associated with Subsonic Turbulent Boundary Layer Flow. J. Fluid Mech., Vol. 28, 1967, p. 719.
- 8. Kistler, A. L.; and Chen, W. S.: The Fluctuating Pressure Field in a Supersonic Turbulent Boundary Layer. J. Fluid Mech., Vol. 16, 1963, p. 41.
- 9. Bendat, J. S.; and Piersol, A. G.: Random Data: Analysis and Measurement Procedures, Wiley-Interscience, New York, 1971.
- 10. Harrje, D. T.; and Reardon, F. H., editors: Liquid Propellant Rocket Combustion Instability. NASA SP-194, 1972.
- 11. Lowson, M. V.: Prediction of Boundary Layer Pressure Fluctuations. AFFDL-TR-167, 1968.

CONT.

HOURIST

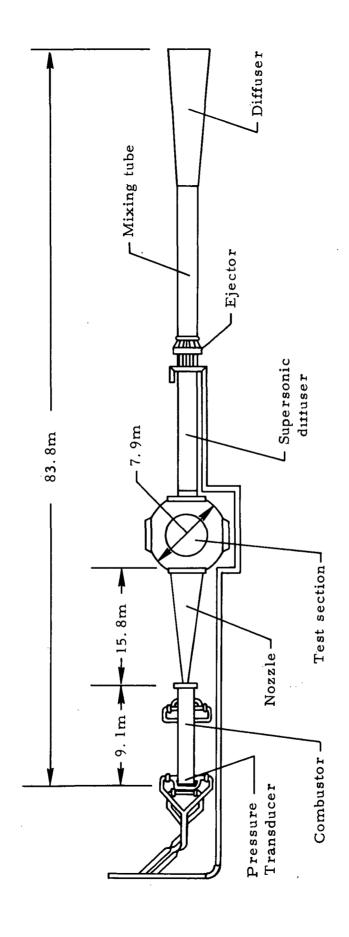
- 12. Houbolts J. C.: On the Estimation of Pressure Fluctuations in Boundary Layers and Wakes. GETIS665D296, General Electric Co., 1966.
- 13. Batchelor, G. K.: The Theory of Homogeneous Turbulence. Cambridge University Press, Cambridge, 1970.
- 14. Hinze, J. O.: Turbulence. McGraw-Hill, New York, 1959.
- 15. Favre, A. J.; Gaviglio, J. J.; and Dumas, R.: Space-Time Double Correlations and Spectra in a Turbulent Boundary Layer. J. Fluid Mech., Vol. 2, 1957, p. 313.
- 16. Favre, A. J.; Gaviglio, J. J.; and Dumas, R.: Further Space-Time Correlations of Velocity in a Turbulent Boundary Layer. J. Fluid Mech., Vol. 3, 1958, p. 344.
- 17. Davies, P. O. A. L.; Fisher, M. J.; and Barratt, M. J.: The Characteristics of Turbulence in the Mixing Region of a Round Jet. J. Fluid Mech., Vol. 15, 1963, p. 337.
- 18. Bies, D. A.: A Review of Flight and Wind Tunnel Measurements of Boundary Layer Pressure Fluctuations and Induced Structural Response. NASA CR-626, 1966.

Momentum Rahickness (mm)	. в	689	902*	3.0Î	. 624	1.89	3.03	2.79	1, 76	1.70	3,48		3.26	2.26
Displacement Thickness (mm)	*9	10.53	8.67	8.92	9.01	10.07	9.15	10.67	13, 10	9.19	7.72		12.19	10.67
Local Mach No.	M_1	5.93	5.74	6.05	5.39	6.15	4,55	4.55	4.96	4.60	4.59		5.78	4.51
Plate Static Pressure 2 N/m	d	8922	1041	1103	1034	2316	5288	6269	12133	Ź68ZI	15029		2958	2116
Local Dynamic Pressure N/m ²	l _b	53,833.9	23.151.5	27, 251, 5	20,276.9	59,040.3	73,950.2	82, 239, 2	202,078.6	184,682.0	207,547.1		66,210.8	47,363.8
Local Velocity (m/s)		1537.1	1574.9	1719.1	646.4	1709.8	1622,4	1859.2	1591.9	1591.3	1839.1		1809.9	1684.7
Model Angle of Attack(deg)	ά	0	0	0	0	0	-15	-15	-15	-15	-15	-15	0	0
Reservoir Temperature Y	$\mathbf{I}_{\mathbf{r}}$	1259	1361	1556	300	1611	1533	1764	1302	1450	1889	1736	1694	1625
Reservoir Pressure S M/m	$P_{\rm r} \times 10^{-6}$	16.966	6.825	6.791	6,515	17.124	6.756	6. 708	16.994	16.821	17.201	17, 145	17, 111	6.894
Run#	!	2	. 2	4	11	12	13	15	18	19	20	24	26	29

TABLE I. Summary of Run Conditions.

Run	P _{tot}	P _u (N/m ²)	P _{bl}	P _{comb}
2	651.8	516.1	135.9	
3	310.8	215.9	94.9	·
4	496.6			122,423
11	88.6	50,2	38.4	8,548
12	748.0	.:583 . 3	134.7	301,957
13	971.1	781.9	189.2	113,751
15	597.1			134,433
18	1724.6	1193.1	531.5	550,141
19	2543.7	2006.2	537.3	1,224,374
20	1660.9	660.7	500.2	290,926
24	1588.6	1080.4	508.2	289,548
26	389.6	230.3	159.3	
29			131.2	

Table II. RMS Values of Fluctuating Pressure Measured in the Combustor and Test Section.



Overall View, 8 Foot High Temperature Structures Tunnel NASA-Langley Research Center. Figure 1.

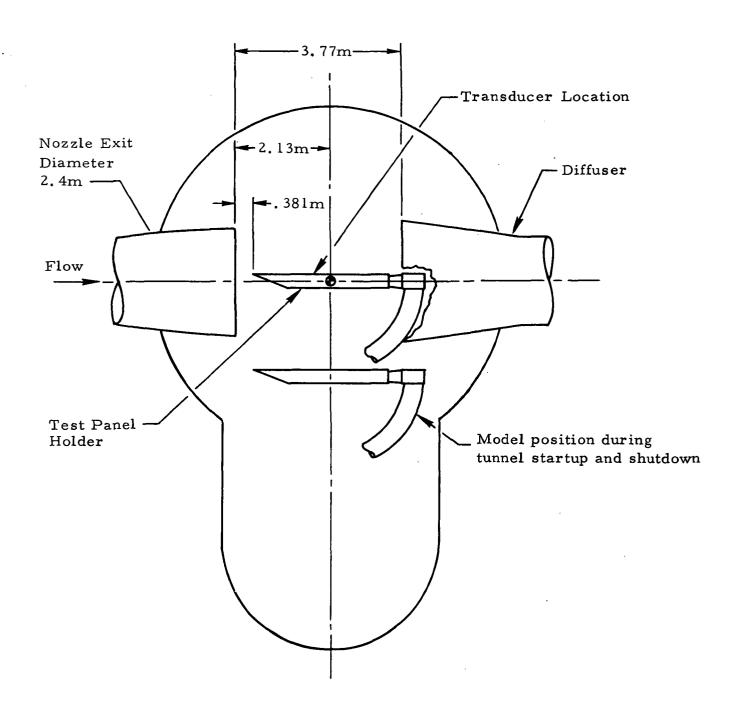


Figure 2. General Configuration of Test Panel Holder and Test Section, 8' HTST.

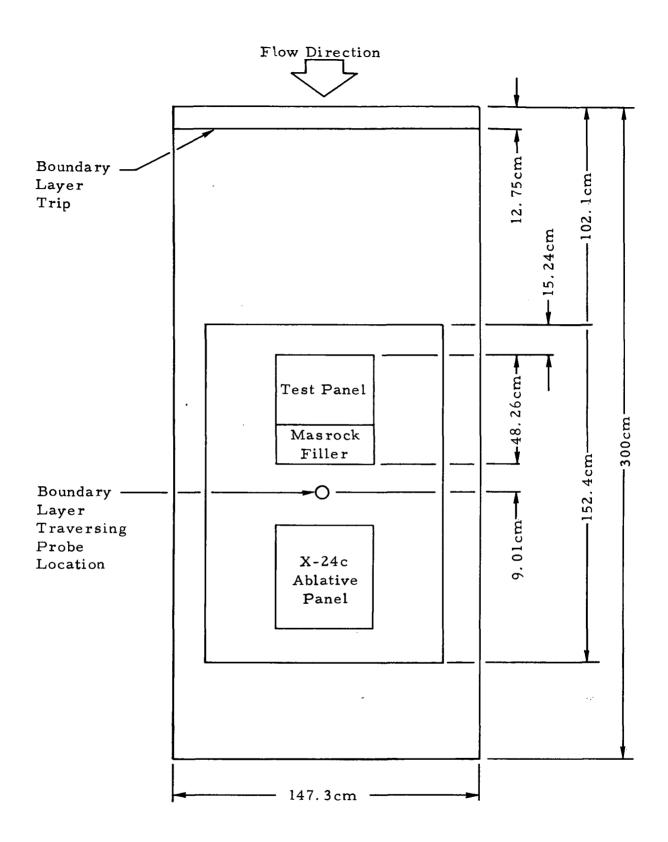


Figure 3. Top View of Panel Holder.

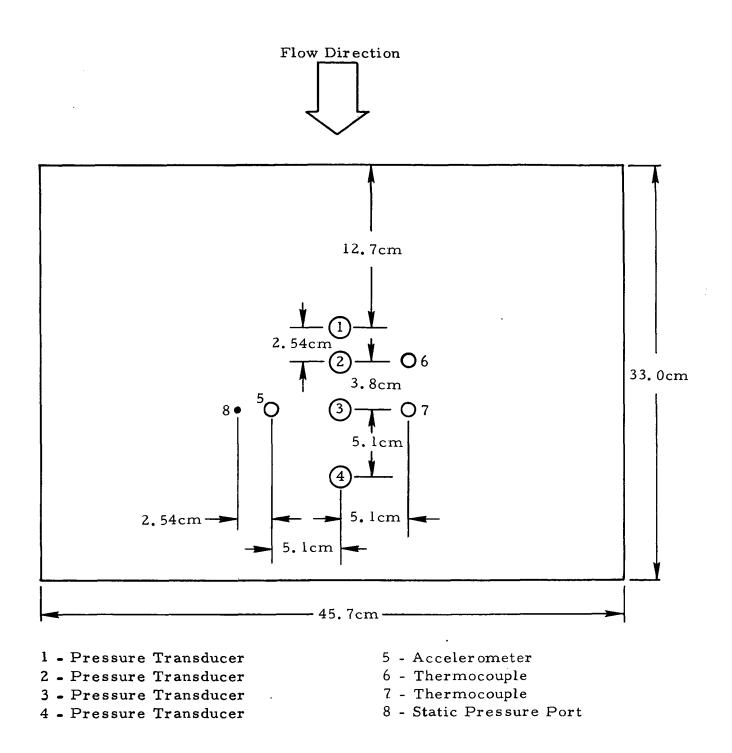
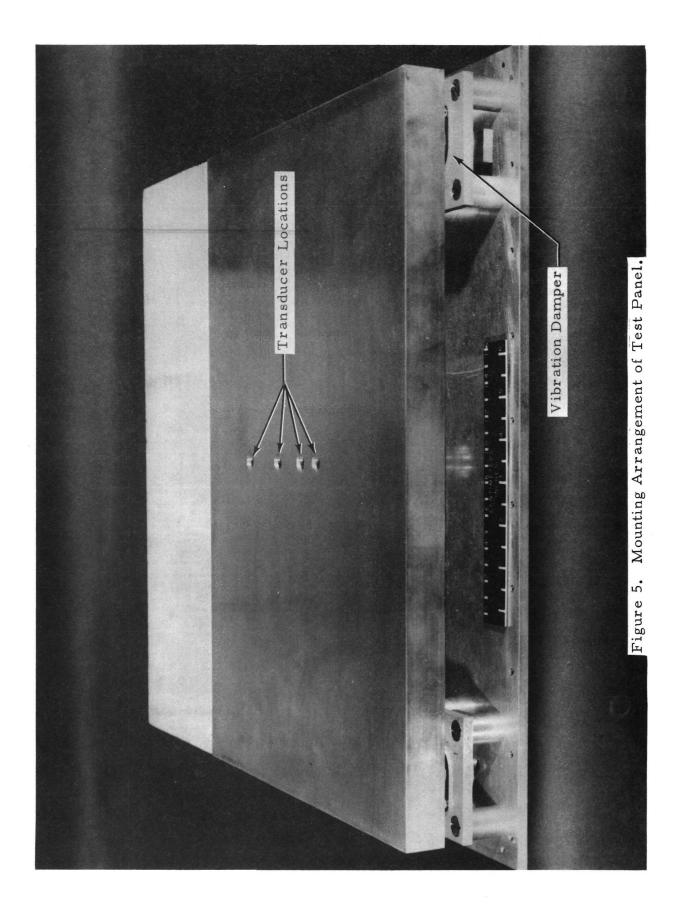


Figure 4. Test Panel Detail and Instrumentation Locations.



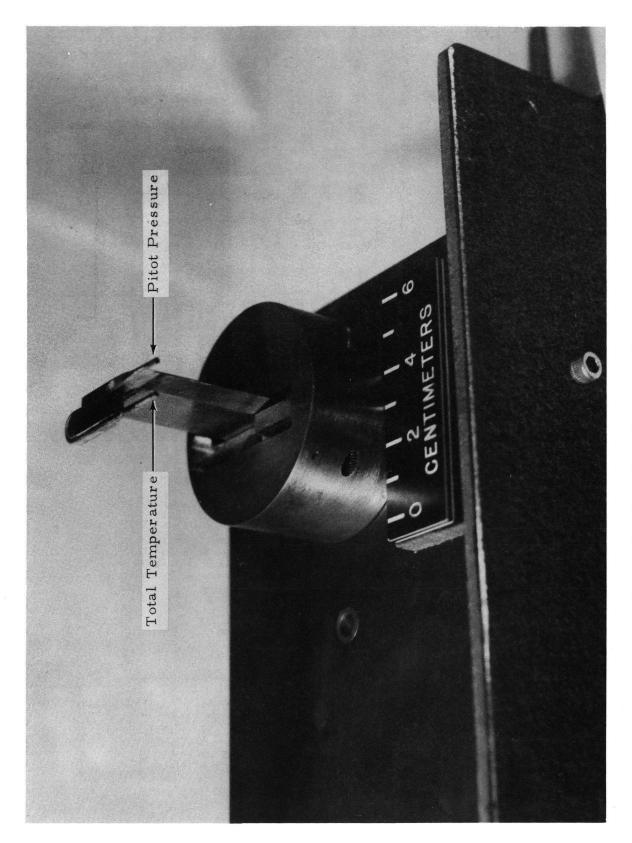
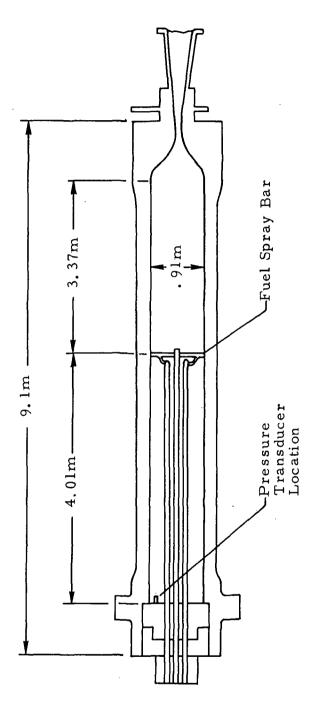


Figure 6. Boundary Layer Probe.



(Drawing not to scale)

Figure 7. Detail of Combustor.

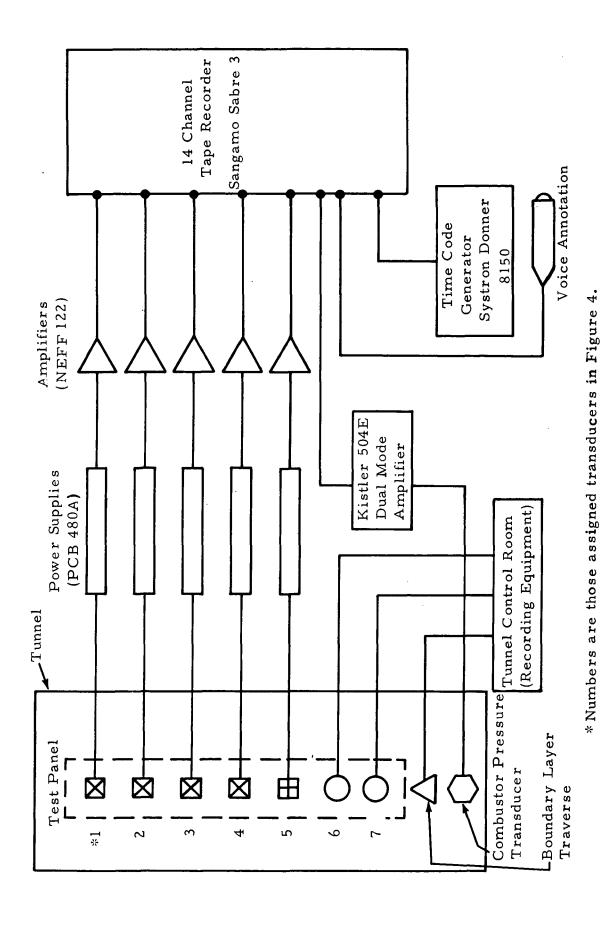


Figure 8. Data Acquisition System.

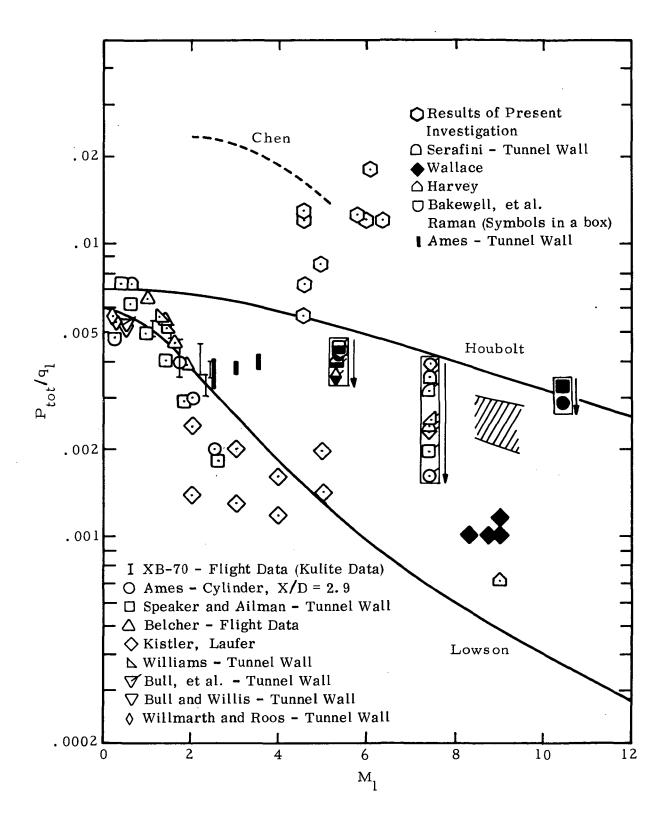


Figure 9. Ratio of rms Pressure to Dynamic Pressure Plotted against Mach Number. Unfiltered Data from Present Investigation.

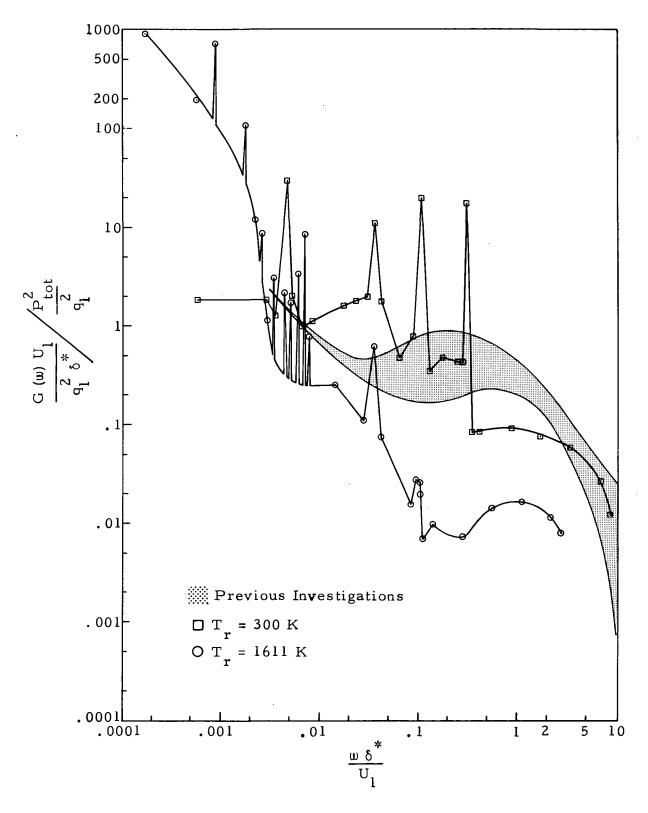
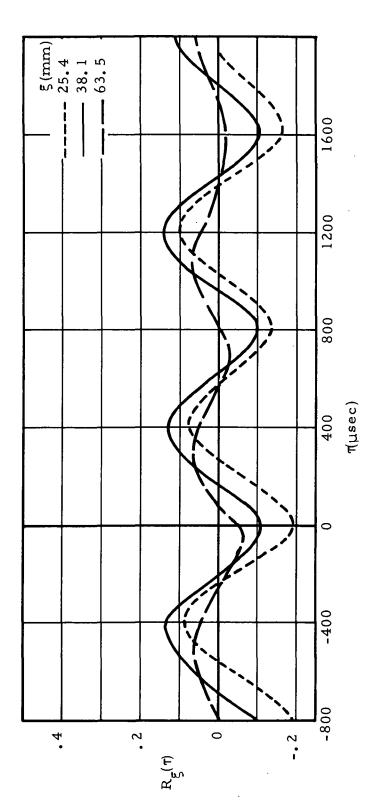
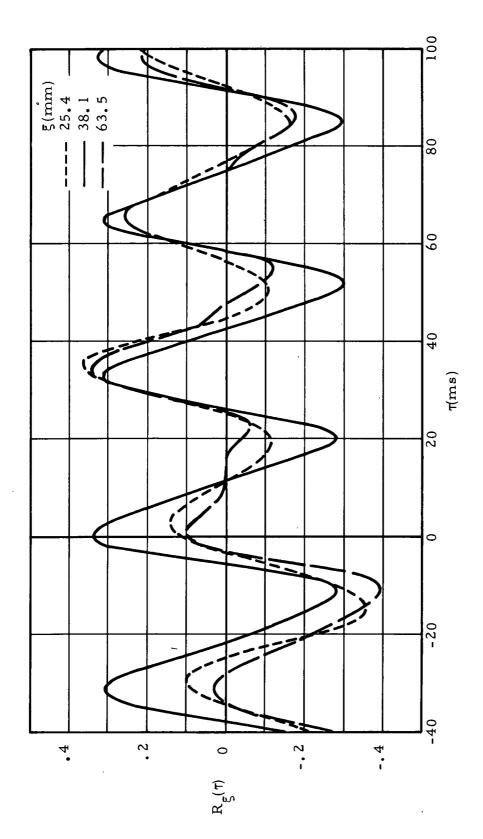


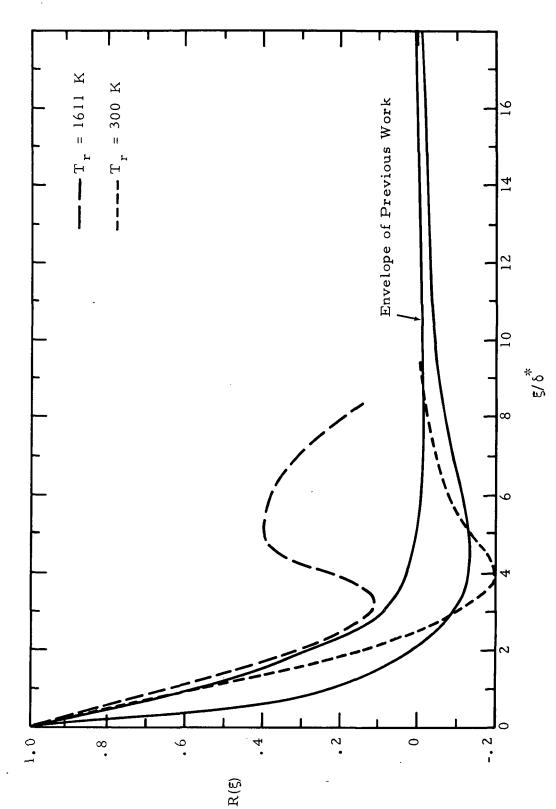
Figure 10. Unfiltered Power Spectra of Pressure Compared with Results of Past Investigations.



Unfiltered Pressure Cross Correlations at Streamwise Transducer Separations 5, Cold Flow ($T_r = 300 \text{ K}$). Figure 11.



Unfiltered Pressure Cross Correlations at Streamwise Transducer Separations ξ ,Run #12 (T $_{\rm r}$ = 1611 K). Figure 12.



Unfiltered Space Correlations of Pressure Compared with Results of Previous Investigations. Figure 13.

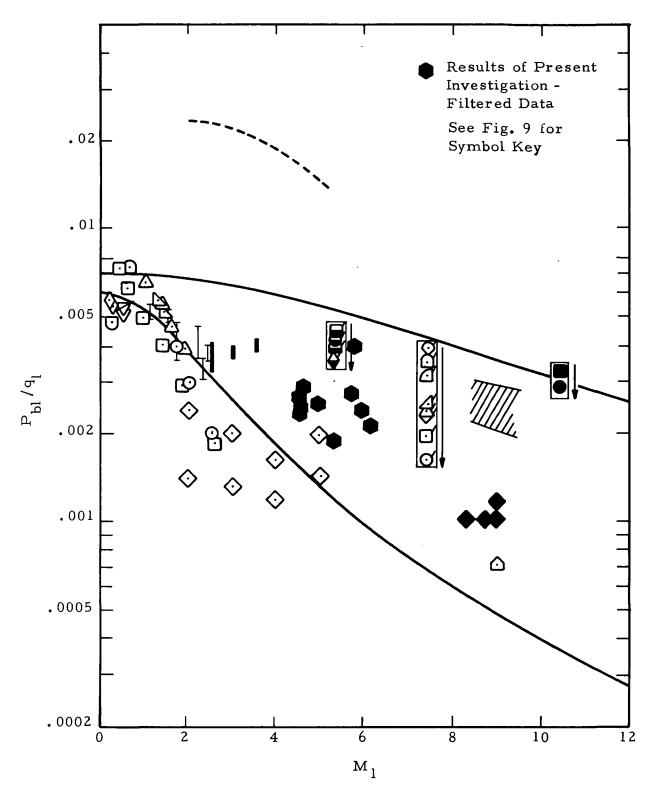


Figure 14. Ratio of rms Pressure to Dynamic Pressure plotted against Mach Number. Pressure High-Pass Filtered at 5 kHz.

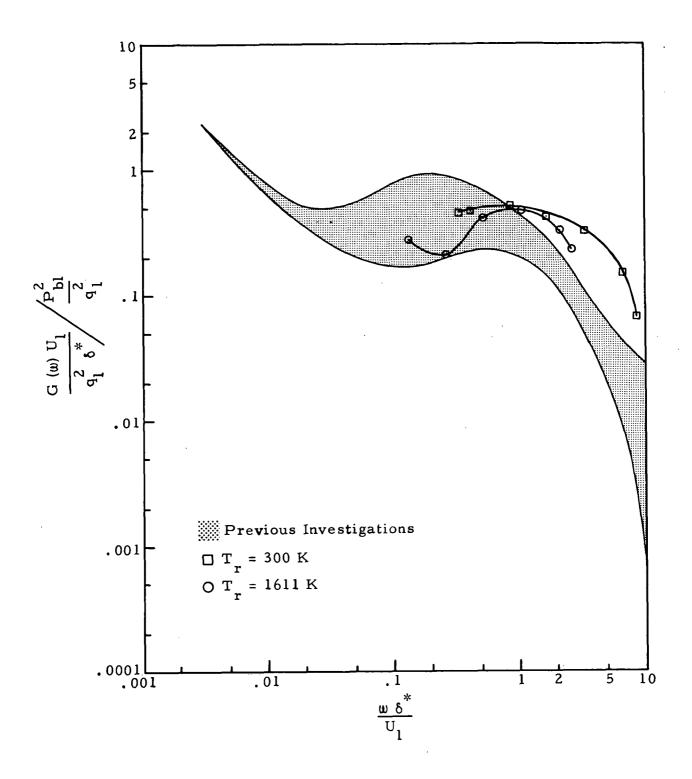


Figure 15. Power Spectra of Pressure High Passed at 5 kHz Compared with Results of Past Investigations.

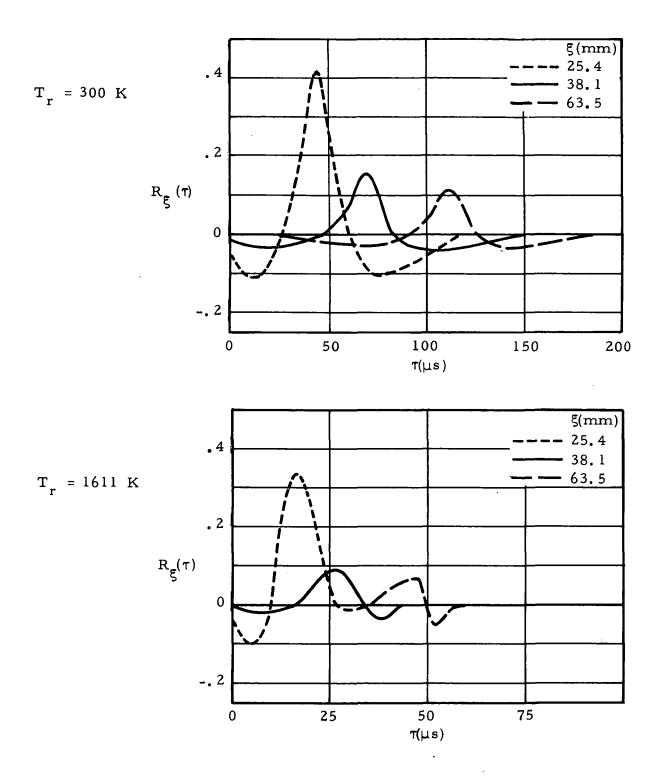


Figure 16. Filtered Pressure Cross Correlations at Streamwise Transducer Separations 5.

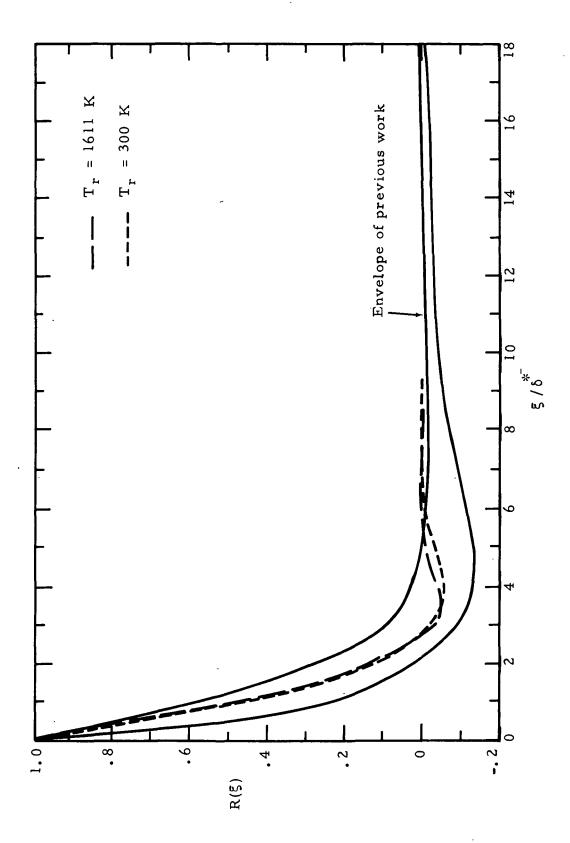


Figure 17. Filtered Space Correlations Compared with Previous Results.

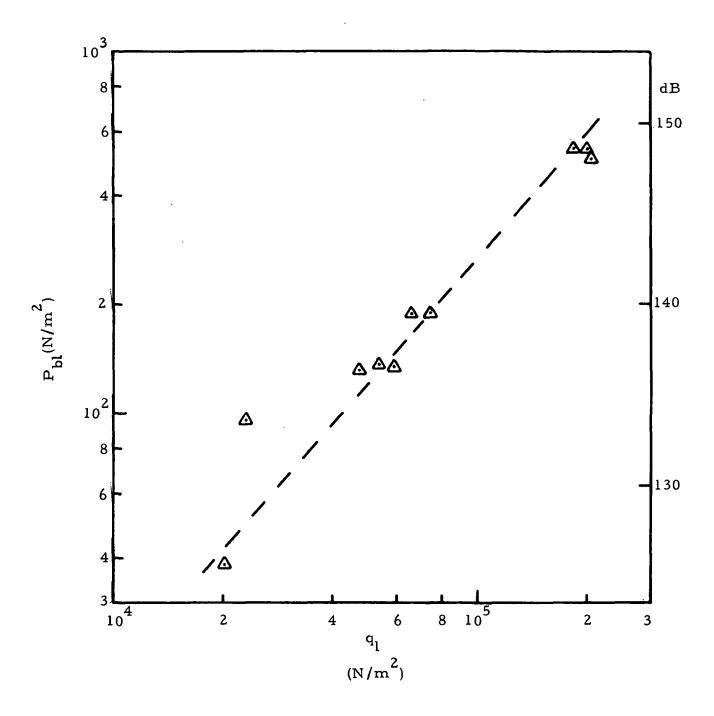


Figure 18. Boundary Layer Pressure (P_{bl}) Versus Local Dynamic Pressure.

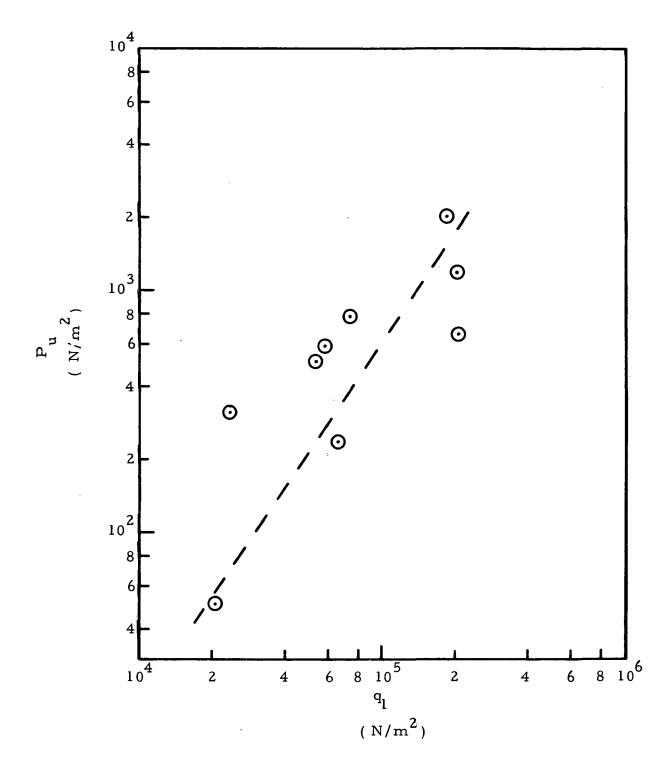
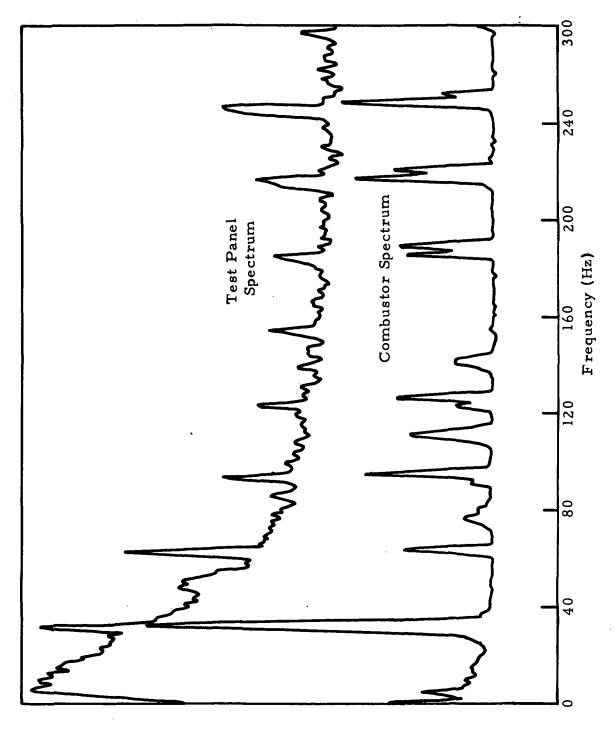
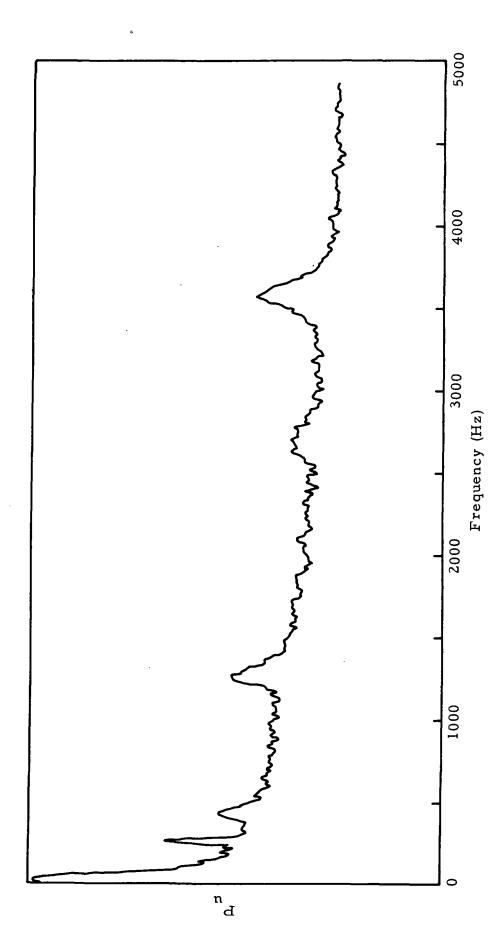


Figure 19. Low Frequency Fluctuation P Versus Local Dynamic Pressure $\mathbf{q}_{\mathbf{l}}$.



Comparison of Pressure Spectra Measured in the Combustor and in the Test Section (Vertical Scale Arbitrary). Figure 20.



Test Panel Spectrum Displaying Presence of Narrow Band Noise in Hot Flow, $T_{r} = 1611 \text{ K}$. Figure 21.

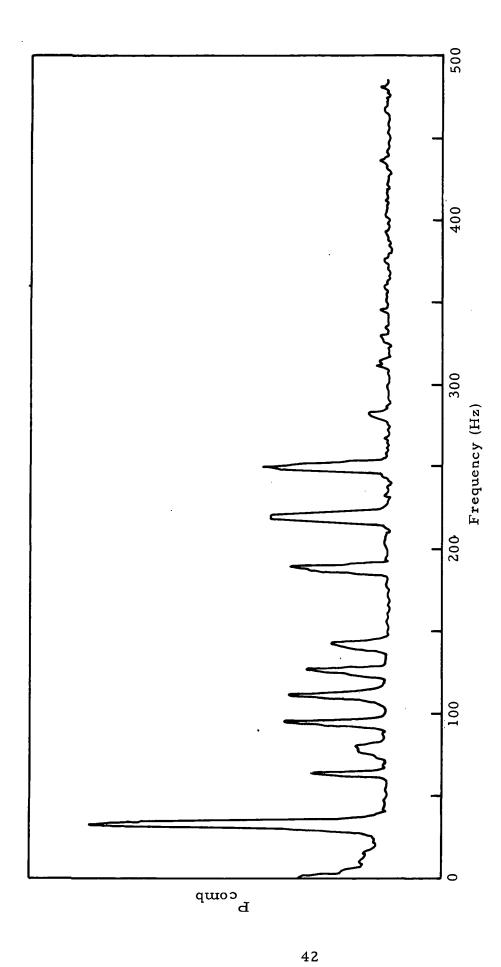


Figure 22. Combustor Spectrum, T = 1611 K.

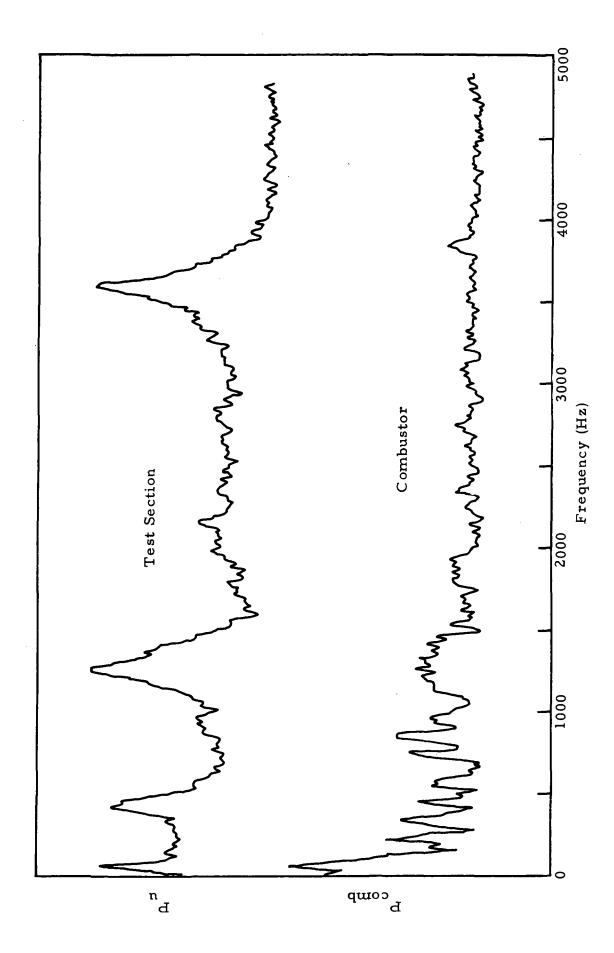


Figure 23. Comparison of Combustor'and Test Section Spectra for Cold Flow, $T_{\rm r}=300~{\rm K.}$

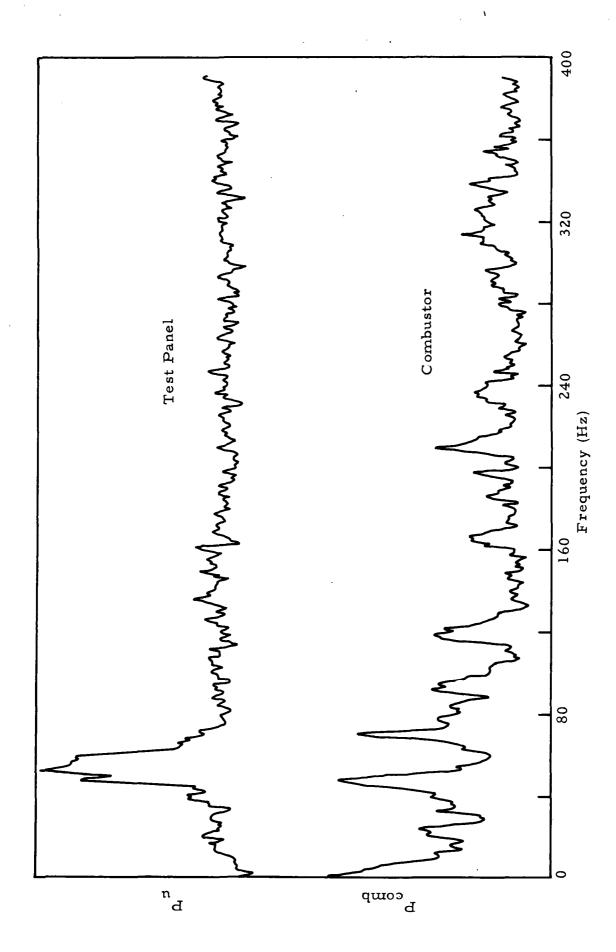
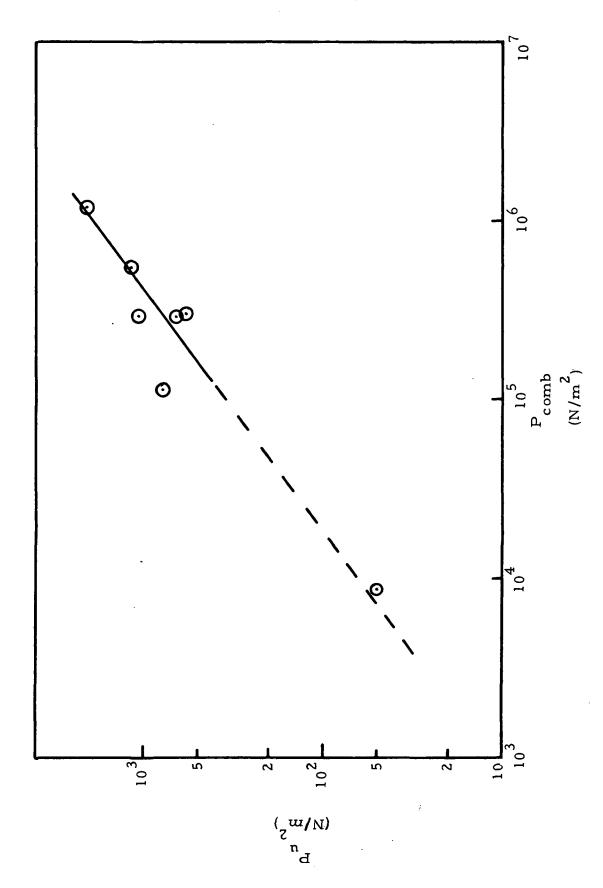


Figure 24. Comparison of Low Frequency Spectra from Combustor and Test Section in Cold Flow, $T_{\rm r}=300~{\rm K}$.



Test Section Pressure Fluctuations below 5 kHz Correlated with Combustor Pressure Variations. Figure 25.

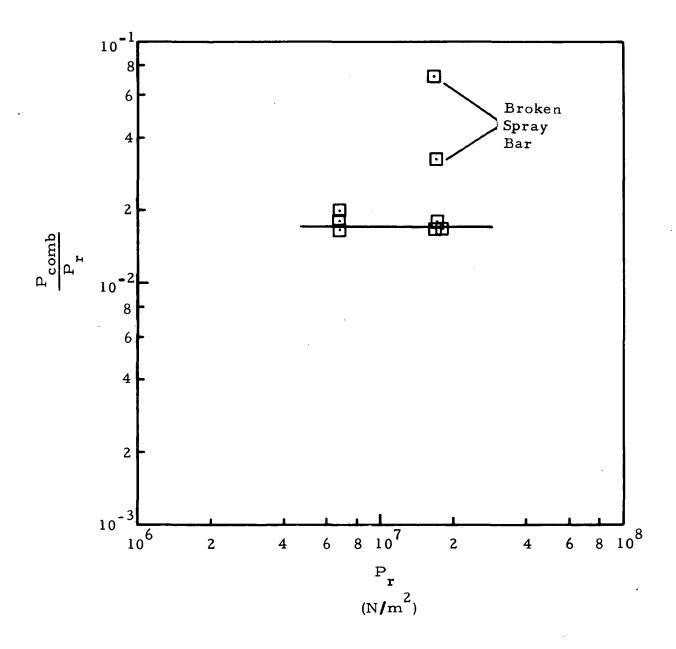


Figure 26. Ratio of Unsteady to Steady Combustor Pressure Fcomb against Steady Combustor Pressure.

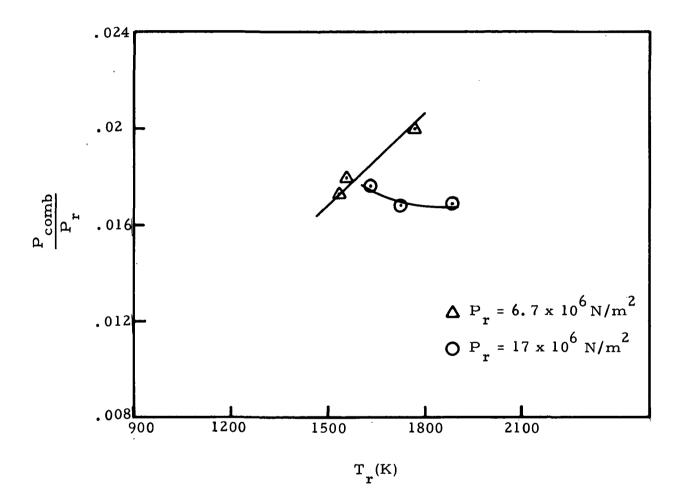
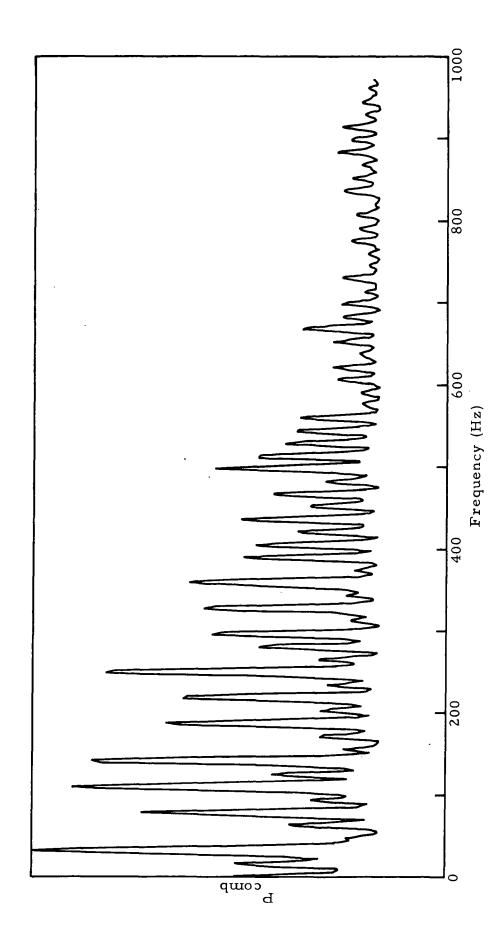


Figure 27. Combustor Pressure Ratio $\frac{P_{comb}}{P_{r}}$ Plotted Versus Combustor Total Temperature.



Combustor Spectrum Measured during Tunnel Operation with a Cracked Fuel Spray Bar, $T_{\rm r}$ = 1450K. Figure 28.

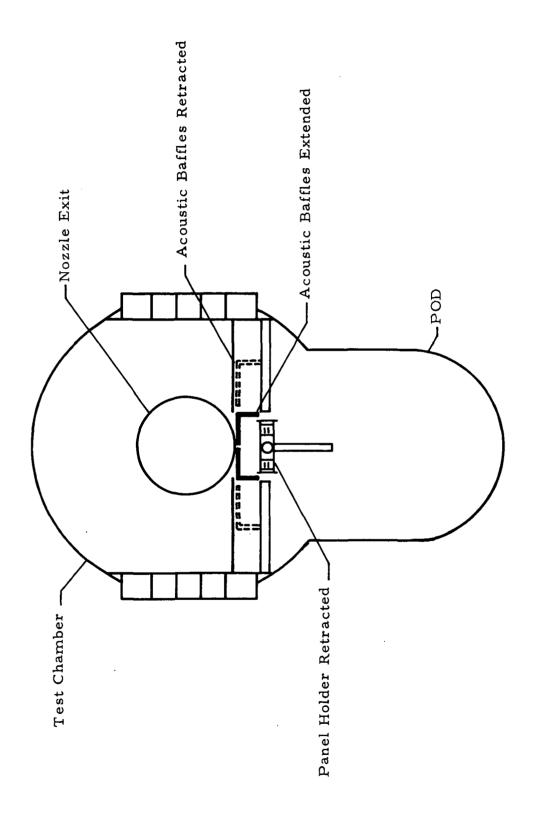
APPENDIX A - MODEL PROTECTION SYSTEM

1

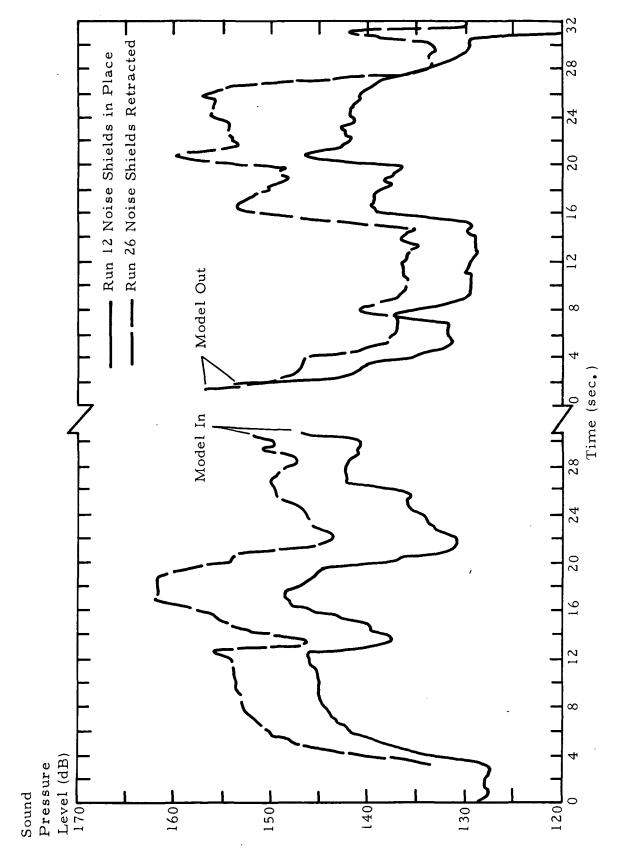
During tunnel startup, and prior to establishment of steady flow conditions in the test section, the model sled remains in the retracted position shown in Figure Al. When test conditions have been established, the model is injected into the stream and data are taken. At the end of a run, the model is retracted, to keep it out of the collapsing flow in the test section as the combustor and ejector are shut off. When it is in the retracted position during the beginning and end of a run, the model sled is protected by two panels covered with sound absorbing material. This material attenuates unsteady pressure loads on the model caused by shock waves and high intensity noise radiation during startup and shutdown. The amount of attenuation this material provides has not been known in the past. As part of the present test program, a secondary study was conducted to measure this attenuation.

Test conditions in Runs 26 and 29 were repeats of Runs 12 and 14, respectively. Startup and shutdown procedures were identical within each pair of matching runs, except that the protective panels did not cover the retracted model in the latter run of the pair. Thus, the full fluctuating loads due to startup and shutdown were experienced by the model. These loads were recorded by the plate pressure transducers and compared with similar recordings made for the runs when the protective panels were in place. These comparisons are shown in Figures A2 and A3, where time histories of the rms pressure fluctuations are shown from the beginning of the combustor countdown to "model in", and then from "model out" to final stop. In the comparison between Runs 12 and 26, it appears that the pressures are attenuated from 8-12 dB by the model protection system. In the comparison between Runs 4 and 29, attenuations are systematically less and average 6-10 dB.

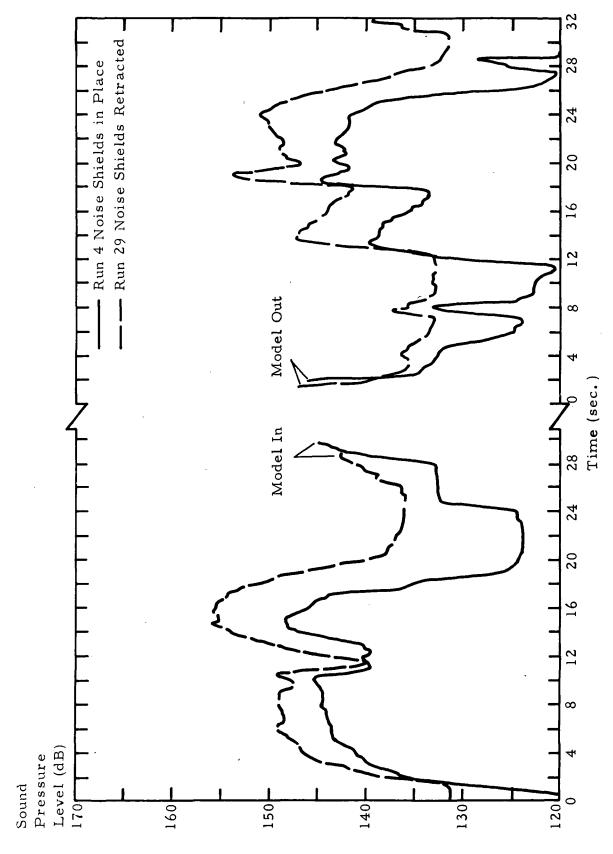
Thus, approximately 6 to 12 dB of attenuation is provided by the model protection system. The fluctuating loads after attenuation are still high (145+dB), but with fair consistency it seems the protective panels reduce the unsteady pressure loads on the model during startup and shutdown to the magnitude of those it will experience in the test section during a test run.



Position of Acoustic Baffles/Model Protection System Figure Al.



Comparison of rms Pressure Time Histories Measured on the Test Panel during Tunnel Startup and Shutdown. Figure A2.



Comparison of rms Pressure Time Histories Measured on the Test Panel during Tunnel Startup and Shutdown. Figure A3.

APPENDIX B

STATISTICAL MEASURES OF A TURBULENT PRESSURE FIELD

RMS Magnitudes. Because the pressure fluctuations are random, it is impossible to predict what their amplitude will be at any specific time. However, over long time periods, measures of the average magnitude can be given which are called the mean-square value and the root-mean-square (rms) value. If p(x,t) is the value of the pressure perturbation at space coordinate x and time t, these average quantities are defined as

$$\frac{1}{p^{2}(x)} = T \xrightarrow{\text{Lim}} \frac{1}{2T} \int_{-T}^{T} \left[p(x,t) \right]^{2} dt$$

$$P_{rms} = \left[p^{2}(x) \right]^{1/2}$$
root-mean-square

The rms value is a measure of the average pressure amplitude, while the mean-square value is a measure of the average energy of the perturbations. Note that both values are strictly defined only in the limit of infinite averaging time. In practice, averaging is done over much shorter times with negligible resultant errors.

In Figure B1, reproduced from Reference 3, a compilation of rms pressure magnitudes measured beneath turbulent boundary layers by previous investigators is displayed. With the exception of one investigation (Chen), the ratio of rms pressure to free stream dynamic pressure is generally found to be on the order of 10^{-3} , with a tendency for this value to decrease with increasing Mach number. The two solid lines are semi-empirical predictions from Referenced 11 and 12.

Power Spectra of Pressure Fluctuations. The power spectral density function of turbulent pressure describes the general frequency composition of the fluctuations in terms of the spectral density of its mean-square value. The mean-square value of the pressure in a frequency range between f and $(f + \Delta f)$ may be obtained by filtering the pressure with a band-pass filter having sharp cutoff characteristics and computing the average of the squared output of the filter. This average squared value will approach an exact mean-square value as the averaging time approaches infinity. The power spectral density function of the pressure measured at location x over the frequency range from f_1 to f_2

is defined by

$$G(f) = \Delta f \xrightarrow{\text{Lim}} \int_{0}^{\frac{1}{2}} \frac{2}{p^{2}} (x, t, f, \Delta f) df$$

It indicates the portion of the total energy in the fluctuations which occurs at frequency f. This function is converted to power spectral density at circular frequency wby the relation

$$G(\hat{\mathbf{w}}) = \frac{G(\mathbf{f})}{2\pi}$$

The integral of the power spectral density function is related to the rms magnitude as

rms =
$$\begin{bmatrix} f_2 \\ f_1 \end{bmatrix} G(f) df$$

In Figure B2, measured power spectra from several previous investigators (References 3 through 8) are plotted. Here the spectra are made nondimensional with the freestream velocity U , the boundary layer displacement thickness δ^* , and the square of the dynamic pressure q_{∞} , and then normalized by the ratio of p^2/q_{∞}^2 . The radian frequency ω (=21f) is made nondimensional by the ratio δ/U_{∞} to account for differing boundary layer time scales in the various experiments. While the low frequency limits of the measurements vary, the shapes of the spectra are similar. All have a broadband character (no discrete frequencies) extending over two or three decades with a sharp roll-off at high frequencies. The low-frequency limits of each data set are established by the background noise levels encountered by each investigator in the wind tunnel used to perform the experiment. Except for Serafini (Reference 5), all investigators have found it advisable to filter out frequencies less than 100 Hz.

Cross-Correlation Function. It is instructive to remember that the turbulent pressure field is intimately related to the turbulent velocity field within the flow. Past hot wire studies in wind tunnels (References 13, 14), boundary layers (References 15, 16), and turbulent jets (Reference 17) have indicated that the velocity perturbations may be thought of as being caused by a convecting, decaying, random pattern of eddies. These whorls of fluid, which are continuously created by mechanisms of fluid instability, travel with the mean flow (though not necessarily at its velocity), gradually losing their identity as the combined influences of shear, viscosity, and molecular diffusion extract and dissipate their energy. Without external inputs of energy into the flow, dissipation of the energy in these perturbations results in a decrease in the

B-3

magnitude of the fluctuations. This is the principle of turbulence reducing screens used in wind tunnels. A turbulent boundary layer extracts energy from the mean flow which borders it. Thus decaying eddies are continuously replaced by new ones created during the process of energy transfer.

It is reasonable to think of each eddy as having an associated pressure perturbation field. As the eddy decays, so must the identity of the pressure field. Thus, again there is the picture of a convecting decaying pattern. The cross-correlation function of the pressure describes both the speed at which the pattern moves, and the rate at which eddies decay and lose their identities. The first characteristic is particularly important because a moving pressure pattern will cause traveling waves in underlying structures. If the wave speed in the structure coincides with the velocity of the pressure field, large structural responses occur, with correspondingly increased fatigue and sound radiation.

The cross-correlation function describes how similar, on the average, the pressure measured at one point is to that measured at another point as a function of the time delay between observations. Consider two measuring points spaced a distance ξ apart in the streamwise direction. If the eddies in a turbulent boundary layer were not decaying, so that a frozen pattern of turbulence was convecting downstream, the exact pattern observed at the upstream station would be observed some time later to pass the downstream station. The difference in times at which the same pattern would be observed at the two stations corresponds to the time of travel between them. This situation could be described by saying that observations at the downstream station are completely similar to, or correlated with, those from the upstream station at a time delay of τ seconds. Here τ is the time of travel and is equal to the observer spacing ξ divided by the convection velocity of the pattern U

$$\tau_{o} = \frac{\xi}{U_{c}}$$

At time differences greater than or less than τ , observations at the down-stream station are not exactly similar to those registered upstream because the upstream observations were of a portion of the pattern which either has not arrived or has already passed.

In the case of decaying, convecting pattern, the concepts of similarity and correlation can still be invoked, but it is apparent that observations at two stations will never be exactly similar. Some decay in the identity of the pattern will always occur between the two points. Thus, at the appropriate value

of T corresponding to time of travel, there will be maximum similarity or correlation, but not perfect correlation.

A mathematical function which gives quantitative form to the concepts of similarity or correlation between two observations at different times is the cross-correlation function. In terms of the pressure p(x,t) measured along streamlines, it can be defined

$$R_{\xi}(\tau) = \frac{\sum_{t=0}^{T} \frac{1}{2T} \int_{-T}^{+T} P(x_1, t) P(x_2, t + \tau) dt}{P_{rms}(x_1) P_{rms}(x_2)}$$

This is a function of the time delay between the signals and its value ranges from 1 (perfect correlation) to 0 (no correlation) to -1 (perfect anti-correlation). In Figures B3 and B4, cross-correlation functions measured beneath turbulent boundary layers in several previous investigations (References 4, 5, 7, 8) are displayed. The individual curves shown on each graph represent the cross-correlation functions between two points at various separations apart. Recalling the picture of a convecting, decaying pattern, a maximum will occur in each cross-correlation function at a time delay corresponding to the pattern's time of travel between them. Because the pattern is decaying, the correlation will not be perfect, so that the maximum correlation takes a value less than 1. Exactly such features are found in these plots. Each is an orderly progression of curves, peaking at successively larger values of time delay that correspond to increased spacing, and thus travel time, between observation points. Further, a continuing decrease in the value of the peak correlation occurs with increasing transducer spacing indicating that the eddies decay more the further they travel. Note also that each correlation function tends to zero rapidly on either side of the peak. This is an indication of the random character of the pressure pattern. Those parts of the pattern which convect past at time delays less than or greater than the travel time must have little or no similarity with parts which cause the maximum or the values of correlation would remain high. This feature of the correlation functions restates the notion that turbulent time histories show no repeatable deterministic features either between experiments or within individual measurements.

The convection speed of the pattern may be determined from these plots by dividing the spacing between observers ξ by the time delay at which maximum correlation occurs. Rate of decay of the pattern eddy may be measured

from the decrease of peak correlation with increasing observer separation.

Space-Correlation Function. Just as the cross-correlation function describes the similarity of observations from two points at different times, the space-correlation function describes the average similarity of observations from two locations at the same time. For two points spaced ξ apart in the streamwise direction this function is defined by

$$R(\xi) = \frac{\lim_{T \to \infty} \frac{1}{2T} \int_{-T}^{+T} P(x_1, t) P(x_2, t) dt}{P_{rms}(x_1) P_{rms}(x_2)}$$

and takes on the same range of values as the cross-correlation function. This function provides information both on the effective area over which the pressure can be said to act coherently (that is, in phase), and on average phase relationships between various locations. Two pressures which are perfectly correlated must necessarily be in phase, while pressures which are perfectly anti-correlated must be 180° out of phase. The intermediate value of zero correlation indicates a random phase relation between the observation points.

Knowing the area over which the pressure is approximately in phase is important since a structure will respond in different manners if it is being forced coherently over a large, rather than small, area of its surface. The way to estimate correlation lengths and areas is best understood from examining actually measured space-correlation functions. In Figure B5, extracted from Reference 1, previously measured space-correlation functions of turbulent pressure are shown for observation points located along lines in the streamwise direction. Here the observer separation ξ has been made nondimensional by the displacement thickness δ to account for the different scale of the boundary layer in each investigation. All of the measured correlations fall rapidly to zero within 4 displacement thicknesses. Most then remain slightly negative for long distances and are asymptotic to a correlation value of zero. A correlation length L can be formally defined by

$$L = \int_{-\infty}^{+\infty} R(\xi) d\xi$$

but this sometimes results in negligible value of L because of the long negative valued "tail" of the correlation function. An alternate, more approximate,

measure of L is twice the distance from $\xi = 0$ to the point where the correlation function crosses zero. By measuring correlation lengths in both the streamwise and transverse direction, their product, called the correlation area, can be calculated. This then gives an approximate area over which the pressure fluctuates in phase since beyond this region the correlation functions are essentially zero, indicating a random pahse relationship.

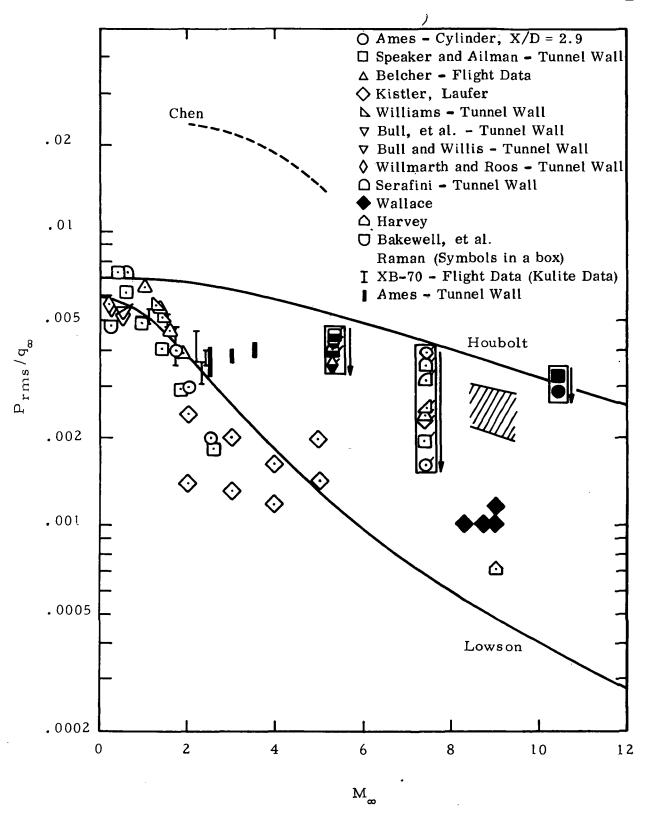


Figure Bl. Ratio of rms Pressure to Dynamic Pressure Plotted against Mach Number. Results of Previous Work.

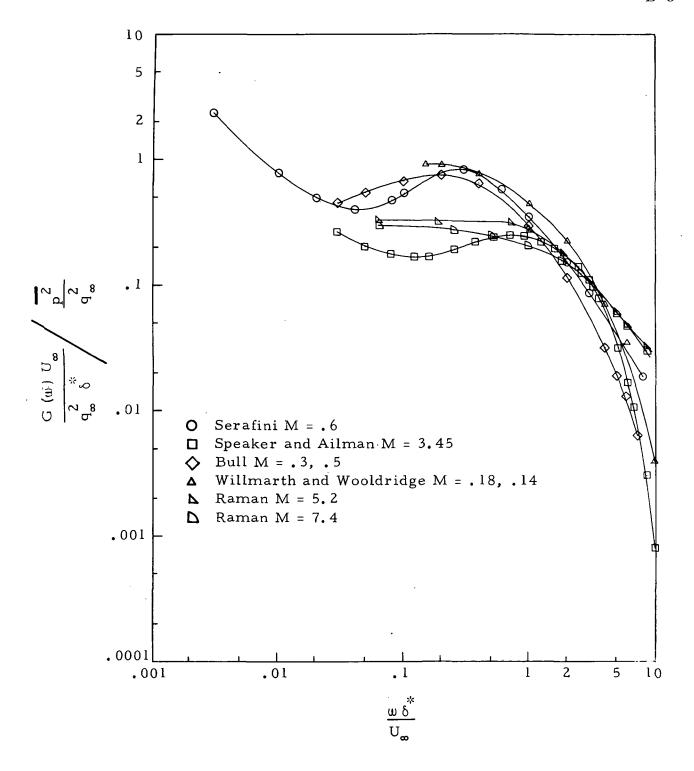


Figure B2. Power Spectra of Pressure Fluctuations from Previous Investigations.

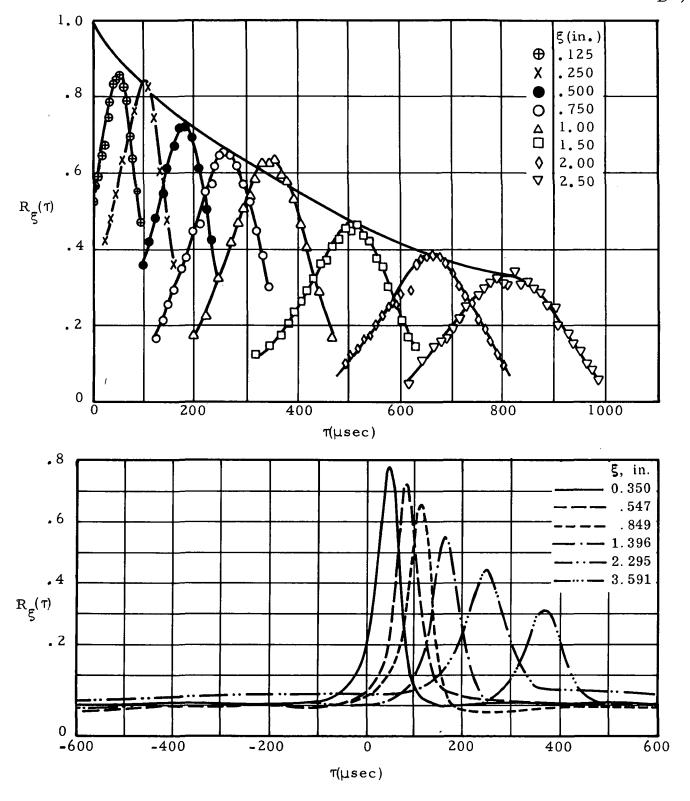
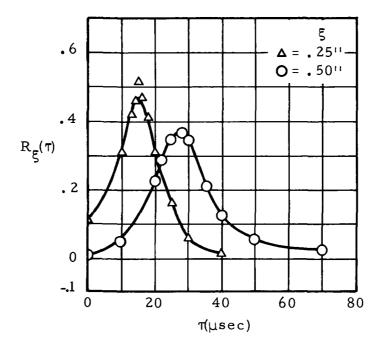


Figure B3. Pressure Cross Correlation beneath Turbulent Boundary Layers at Various Transducer Separations § Top: Bull; Bottom: Serafini.



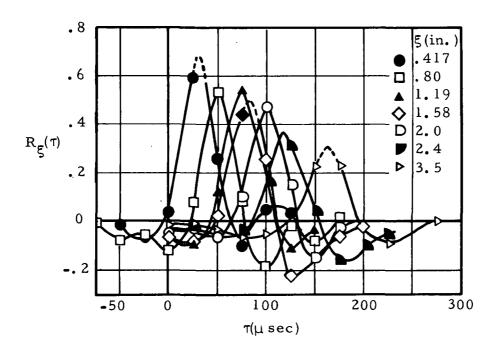


Figure B4. Pressure Cross Correlation beneath Turbulent Boundary Layers at Various Transducer Separations, ξ, Top: Kistler and Chen; Bottom: Speaker and Ailman.

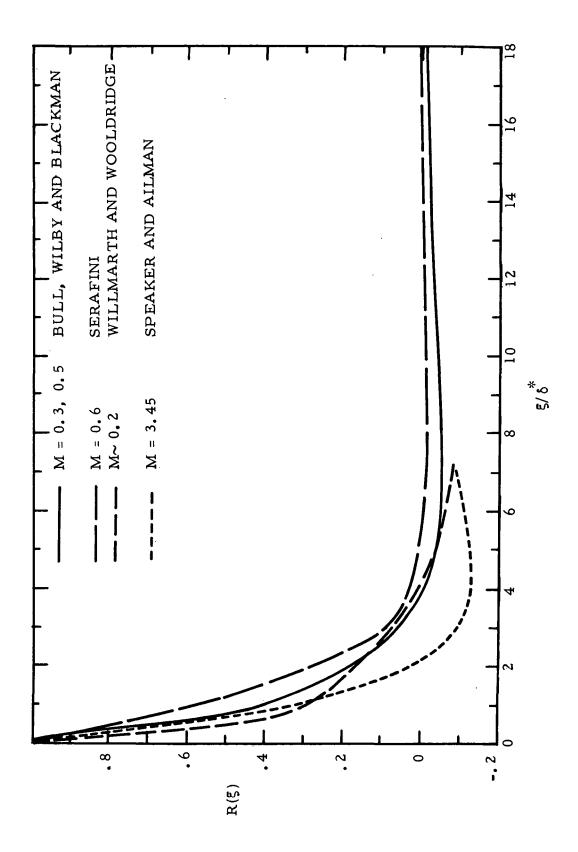


Figure B5. Pressure Space Correlation from Previous Investigations.